Molecular Dynamics Simulation Study of PEO-based Polymer Electrolytes in Aqueous Solution

By

Zhi Tao

Dissertation

Submitted to the Faculty of the

Graduate School of Vanderbilt University

In partial fulfillment of the requirements

For the degree of

DOCTOR OF PHILOSOPHY

In

Chemical Engineering

05-2008

Nashville, Tennessee

Approved

Professor Peter.T.Cummings

Professor Martin.Douglas.Levan

Professor Kane.G.Jennings

Professor Clare.M.McCabe

Professor Deyu.Li

TABLE OF CONTENTS

ACKNOWLEDGEMENTS

More than five years ago, I decided to come to the United States to become a graduate student and extend my expertise in chemical engineering. I was lucky to choose Vanderbilt University, where I spent happy time on the campus and met great people I will always remember.

First and foremost, I would like to thank my advisor, Prof. Peter T. Cummings, for having the patience listening to my problems and repeatedly setting me back on the right course of research when I lost direction.

This dissertation is the result of multi-disciplinary joint effort and would not be possible without help and advice from experts working outside my field. I am especially thankful to Dr. Simonson from Oak Ridge National Laboratory for providing me valuable experimental data and useful comments. I also greatly appreciate moral and technical support I received from my fellow members of Cummings's group during the past five years.

Last but not least, I would like to acknowledge the members of my dissertation committee: Prof. Kane G. Jennings, Prof. M. Douglas. LeVan, Prof. Deyu Li, and Prof. Clare McCabe, whose guidance through all the stages of my Ph.D. research was extremely helpful.

LIST OF FIGURES

LIST OF TABLES

CHAPTER I

1 INTRODUCTION

Energy is crucial to many aspects of our life. Energy generation and storage are growing topics in the field of academic research and industrial applications due to the rapidly growing energy demand of the modern world. There are many different forms of energy sources which can be classified to the following categories:

- **Fossil fuels**: defined as fuel formed from the organic remains of prehistoric plants and animals, such as coal, natural gas and oil. The major and important drawback of fossil fuels is production of carbon-dioxide as the by-product of burning fossil fuels. Carbon-dioxide is strongly implicated in causing "the greenhouse effect", a severe environmental problem reflected in the warming of the earth. Another major drawback of fossil fuels is that they are not renewable, since the geological processes to convert organic materials to fuel take 10^6-10^9 years. However, taken as a whole, the fossil fuel inventory will last several centuries [1].
- **Renewable energy**: given that fossil fuels are not renewable sources of

energy, there is increasing interest in the generation of energy from renewable resources, such as solar power, water power, wind and wave power or from renewable bio-materials. Currently renewable energy is actually limited to small–scale power generation only [2].

- **Nuclear power**: a type of nuclear technology used to generate energy through nuclear fission. For a given amount of fuel, it produces much more power than other energy sources but the nuclear waste generated is hazardous, with no consensus yet reached to date on the best way to store or dispose of it.

Many renewable energy sources (e.g., solar and wind) are characterized by periods of production (e.g., daylight and blowing winds, respectively) followed by non-production (e.g., night and no wind, respectively). Hence, *energy storage* is a key to making energy continuously available, as well as in many cases making energy portable (e.g., for electric or hybrid vehicles). A battery is a device used to store energy in an electrochemical form. Every battery has a positive electrode (cathode) and a negative electrode (anode), which are immersed in a solid or liquid electrolyte. All materials are enclosed in a container with a separator between the electrodes to keep them apart. Batteries are usually divided into two main classes: Primary batteries (disposable batteries which are intended to be used once and discarded) and secondary batteries (rechargeable batteries which can be recharged by applying electrical current).

In this work we use molecular dynamics simulation to understand how polymer batteries, one of the most widely used secondary batteries, could be optimized for more efficiency.

Most polymer batteries are lithium polymer batteries (LPBs) that use lithium-ion-conducting solid polymer electrolytes (SPEs) defined as lithium ions dissolved in a polymer host. LPBs have several outstanding advantages compared to other common batteries: (i) since lithium is the lightest and smallest metal, they have the potential to yield high energy density, e.g., polymer electrolytes can be shaped into extremely thin films with large surface area giving high energy density (> 100 W/dm^3) (ii) non-flammability of the lithium based polymer electrolyte provides safety even at extreme conditions, and (iii) because no metal battery cell casing is needed, the batteries can be formed to any desired shape and size. Due to these favorable properties, LPBs can be, and are being, used in a wide range of applications, such as portable electronics, medical equipment, and hybrid vehicles[3, 4].

The industrial importance of the LPBs has created the need for fundamental research which would provide the theoretical basis for the design of new polymer batteries with improved performance. The currently used polymer electrolytes, the major component of polymer batteries, have many deficiencies. One of the major disadvantages is the low conductivity at room temperature [3]. Therefore, there is a need to explore new polymer electrolytes

with increased ionic conductivity. The main effort to date has been directed towards understanding the electrochemical properties of the systems, with a particular interest in understanding the ion-transport mechanisms. It has been well established that most ions carrying electric current are transported through the amorphous regions of polymer, and that the transport of ions is largely controlled by the interactions between ions and polymer [3, 4]. To date, however, our understanding of the microscopic structure and dynamics of ions in their polymer hosts is still incomplete.

Polyethylene oxide (PEO) is the most popularly used polymer host for polymer batteries. The majority of experimental and computer simulation studies to date have focused on PEO/Ions or PEO/water binary mixtures and have reported many promising results, showing that cations can move in the amorphous phase of the polymer matrix and ion movement is directly related to the interaction between ions and polymer host [5-10]. However, recent experimental studies have shown that ternary mixtures with polymer electrolytes in water solution can provide even more attractive properties than binary polymer-salt systems [11]. Water has a dramatic influence on the structural environment of lithium ions in the polymer matrix and the mobility of ions as a consequence of structural changes [11]. In an effort to better understand LPB systems we are going to use molecular dynamics simulation (MD) to investigate two aspects of LPB systems: the microscopic structure and dynamics of the

electrolyte, and the influence of water as a third component in the system. Understanding these two phenomena could provide the theoretical understanding for the development of polymer batteries with improved performance, especially increased ionic conductivity. As a simulation model system we choose an electrolyte containing lithium ions and polyethylene oxide (PEO). To accurately describe interactions between all components in the mixture, we will develop a polarizable forcefield, which we will show to be a key factor in increasing the accuracy of molecular dynamics simulations of these systems.

The remainder of the thesis is organized as follows. In chapter 2 we provide an overview of solid polymer electrolytes, the components of typical polymer electrolytes, the conductivity mechanism and the experimental and simulation methods used to study polymer electrolytes along with relevant results are discussed. In chapter 3, after describing molecular dynamics (MD) simulation, we review recent developments of forcefields and describe methods to treat polarization effects. In chapter 4, we describe our work on the development of a polarizable forcefield and the methodology of our molecular dynamics simulations. Then, we will present and discuss the results from our MD simulations and compare them with available experimental data. Finally conclusions are drawn and possible future work is discussed in chapter 5.

CHAPTER II

2 BACKGROUND

In this chapter, we will introduce the basic concepts of polymer electrolytes and their role in polymer batteries, followed by the description of the composition of polymer electrolytes, the polymer matrix and inorganic salts. We will then discuss the mechanism of ionic conduction. Finally, we will describe available experimental methods from which we can get data to compare with our molecular dynamics simulation results.

2.1 Solid Polymer Electrolytes

Mixtures of polymers and salts have proven conducting properties and have the potential to be used as a new class of solid electrolyte for energy storage applications. This fact underlies the design of lithium polymer batteries, which use an ion-conducting polymer instead of the traditional combination of a microporous separator and a liquid electrolyte. The use of thin polymer electrolytes can increase safety compared with traditionally used liquid electrolytes. In the process of designing a successful polymer electrolyte (PE), many factors have to be carefully considered [4]:

- **Ionic conductivity at room temperature**: PEs should have an ionic conductivity in the range 10^{-2}-10^{-3}S/cm (a lower value may work for some practical applications; the minimum useful value is 10^{-5}S/cm).
- **Compatibility**: PEs must be chemically and electrochemically compatible with electrode materials.
- **Thermal stability**: PEs must be thermally stable in contact with electrodes.
- **Mechanical stability**: PEs must be mechanically stable in order to be scaled up from the laboratory to full production.
- **Commercial availability**: PEs should be inexpensive and readily available.

A solid polymer electrolyte (SPE) is defined as a solvent-free system with the ionic conducting phase formed by dissolved salts in a polar polymer matrix [3, 4]. SPEs have three important functions in polymer electrolyte batteries: (i) they carry cations (mostly lithium ions) and they also can be formed as thin films to increase the energy density; (ii) they work as an electrode spacer eliminating the need to incorporate an insert porous separator, and (iii) SPEs can provide good electrical contact with electrodes, which means they do not need to be in the liquid phase [3, 4].

Figure 1 shows a schematic representation of a typical lithium-based polymer battery. The anode is formed by a carbon-Li intercalcation compound,

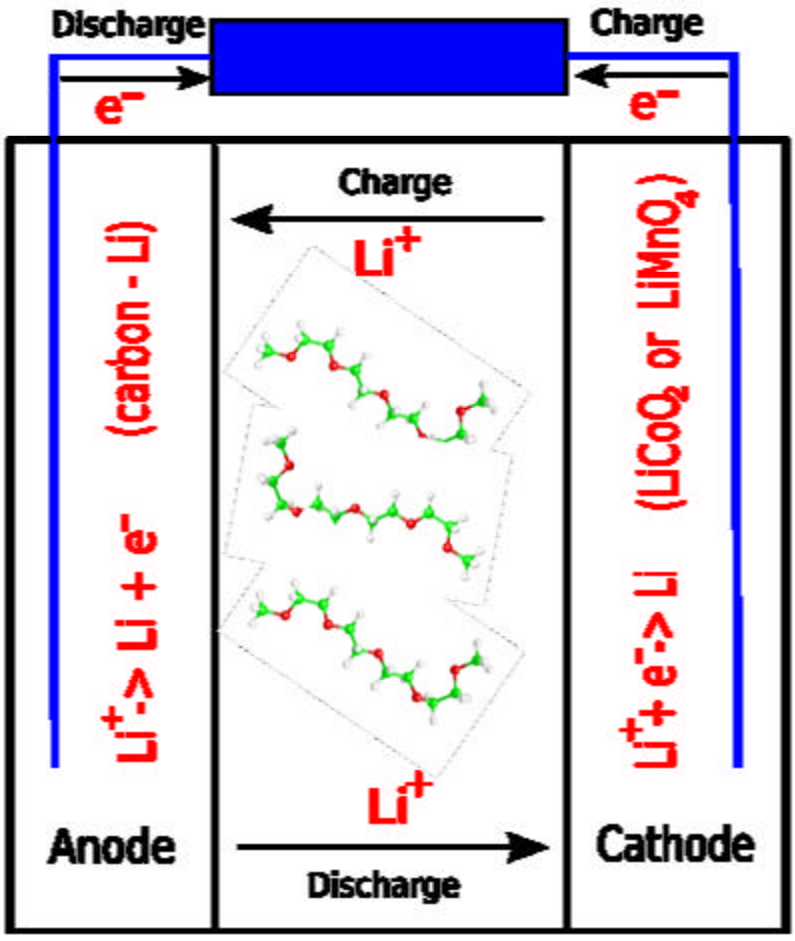

Figure 1: A schematic drawing of a typical Li-polymer battery [13].

the cathode is formed by lithium salts, most in the format of $LiCoO_2$ or $LiMn_2O_4$, and the space between them is filled with a ion-conducting polymer-electrolyte solution instead of the traditional liquid electrolytes [13]. During a discharging process, a typical reaction at the carbon anode is the oxidation of intercallated Li and its realease into the solution where it conducts charge. At the cathode Li ions are reduced and incorporated in $LiCoO_2$ or $LiMn_2O_4$ compounds. During charging the processes are reverted.

Unfortunately, solid polymer electrolytes have limitations especially at room temperature; exhibiting ionic conductivity of the order of 100 to 1000 times lower than other materials [4]. Therefore, considerable research has been devoted to compensation of this drawback so that they work effectively at ambient temperature and to understanding the conductivity mechanism.

In the following sections, we now describe each component of the polymer batteries.

2.2 Polymer host

In polymer electrolytes, the polymer host works both as an electrolyte and as separator isolating the electrodes. A successful polymer candidate should satisfy the following requirements [3, 4, 15]:

- The polymer must contain atoms or groups with sufficient electron donor power to form co-ordination bonds with cations. For alkali ions, such as

lithium, oxygen is regarded as the preferred electron donor

- The polymer must have a suitable distance between coordinating sites to allow the formation of multiple intra-polymer bonds for good solubility of cations.
- The polymer should have low barriers to bond rotation to facilitate ion motion

Potential candidates for a polymer host are [3]:

poly (methylene oxide) $(-CH_2O-)_n$, poly (ethylene oxide) $(-CH_2CH_2O-)_n$, poly (trimethylene oxide) $(-CH_2CH_2CH_2O-)_n$, poly (propylene oxide) $(-CH_2CH_2(CH_3)O-)_n$, and poly (ethylene imine) $(-CH_2CH_2NH-)_m$.

The first of these, poly (methylene oxide), $-(CH_2-O)_n$, has a relatively rigid chain [3], while the third, poly (trimethylene oxide), $-(CH_2-CH_2-CH_2-O)_m$, is unable to adopt low-energy conformations [3].

PPO is the second most extensively used polymer in polymer electrolyte studies after PEO. Unlike PEO which has coexisting amorphous and crystalline phases, PPO is completely amorphous. However, at higher temperature, e.g., higher than 60-80^oC, PPO/salt systems display appreciably lower conductivities than those measured under the same conditions for PEO/salt complexes, caused by the steric hindrance from the pendant methyl group [3].

Finally PEI is a product of the cationic polymerization of the ethylene imine or the cationic ring-opening polymerization of aziridene. It is highly

hygroscopic and, unlike PEO or PPO, can also form hydrogen bonds (N-H…N) between polymer chains. In anhydrous state, these hydrogen bonds lead to the formation of double-stranded helical chains, which can decrease the ionic conductivity [3].

As a result, neither of them can be used as polymer electrolytes, with most SPEs being based on the commercially available polyethylene oxide (PEO) polymer [3]. PEO has very good solvating properties for a wide variety of salts, due to the interaction of its ether oxygen with cations. The chemical structure of PEO explains most of the properties of this polymer host. Figure 2 shows the structure of 1, 2-dimethoxyethane (DME), the shortest and simplest ether molecule having the local conformational properties of PEO [14, 16]. A segment of a long PEO polymer chain is shown in Figure 3 [15].

The melting point of PEO is a function of the average molecular weight and molecular weight distribution of the sample. Usually, it varies from 60^{o}C for lower molecular weights (~4000 g/mol) to 66^{o}C for bigger molecular weights (~100,000g/mol) [3]. The glass transition temperature (T_g) also displays a close relationship with molecular weight, it grows up to a value of -17^{o}C of a molecular weight 6000g/mol [17]. Values of -65 and -60^{o}C are reported for higher molecular weight samples [3]. PEO is completely soluble at room temperature in water and also soluble in a wide range of common organic solvents [18]. PEO and most PEO/salt mixtures exhibit co-existence between

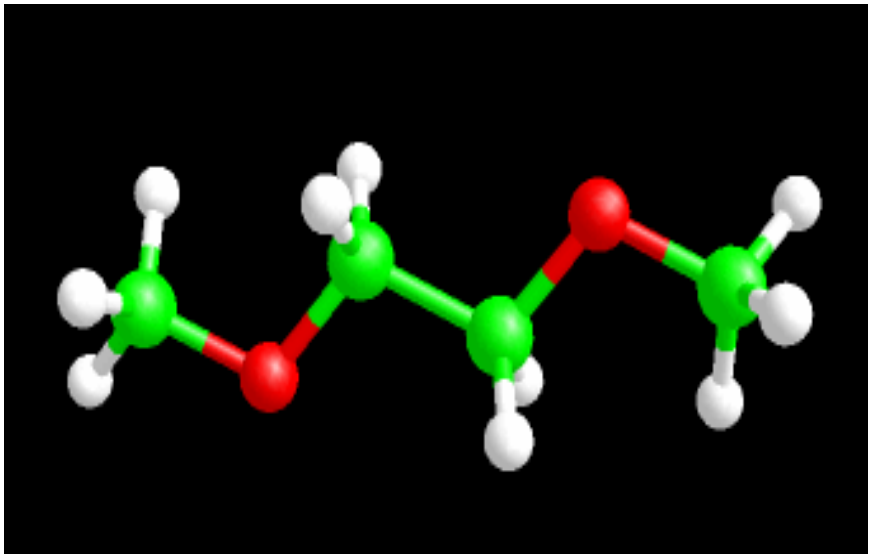

Figure 2: The structure of DME: CH_3-O-CH_2-CH_2-O-CH_3. The green, red and white spheres represent carbon, oxygen and hydrogen atoms respectively [16].

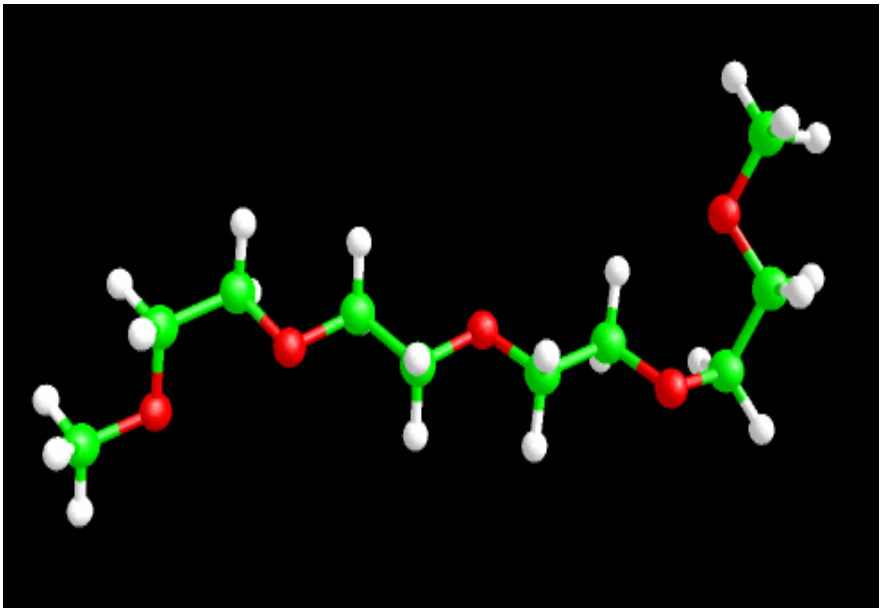

Figure 3: A segment of a polyethylene oxide chain [15].

crystalline and amorphous phases; in fact only 15-30% of PEO is in the amorphous phase at room temperature [14]. The unit structure of crystalline PEO has been well established from x-rays and neutron scattering experiments [14, 15, 19]. As shown in Figure 4, it contains four helical chains in a cell. Each chain has a helical structure with repeating - (CH_2 - CH_2 - O) – units [14, 15, 19].

Neutron scattering has proven to be very promising in determining the PEO polymer melt structure [20, 21]. For example, Annis and coworkers studied the structure of a PEO polymer melt using neutron scattering experiments [20, 21]. On the theoretical side, recently Lin *et al.* and other researchers reported a series of molecular dynamics simulations of the amorphous regions of the PEO polymer [15]. Their simulation results were found to be in good agreement with experiments [15].

When operated at room temperature, at which PEO displays a large degree of crystallinity (a major barrier to ions transport), polymer electrolytes always end up with an undesirably low ionic conductivity. For example, polymer electrolyte systems (PEO/LiX) give an ionic conductivity of the order of 10^{-6}S/cm at ambient temperature. Therefore current research efforts to develop batteries with better performance resulting from higher ionic conductivity are mainly focused on lowering the degree of polymer crystallinity under ambient temperature by using lithium salts with large anions or by adding

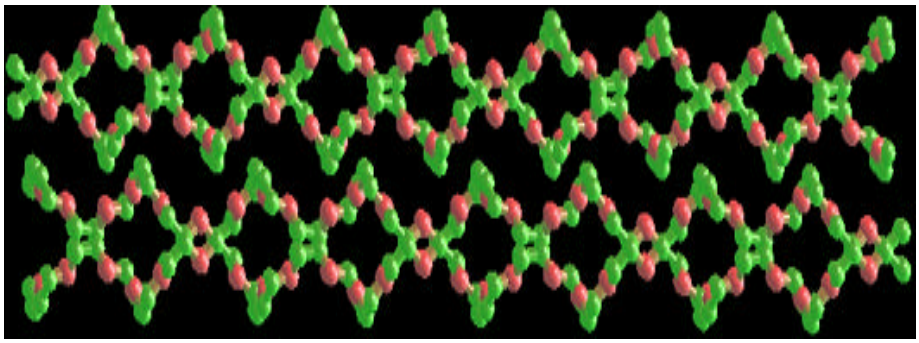

Figure 4: Schematic representation of crystalline PEO unit cell. Hydrogen atoms are not shown here for clarity [19]

low molecular weight liquid plasticizers [12]. In addition, for some polymer/salt electrolytes, such as PEO/$LiSbF_6$, high ionic conductivity in the crystalline polymer phase was found indicating that cations can also diffuse in the crystalline phase of polymer [22]. Also, recent studies have shown that composite polymer electrolytes with ceramic fillers can offer batteries with better performance, improved compatibility and safety [12].

2.3 Thermodynamics of polymer-ion solvation

A salt dissolved in a polymer solvent will decrease the free energy of the system because of changes in both enthalpy and entropy, as shown in the equation below:

$$\Delta G_{mixing} = (\Delta H_{mixing} - T\Delta S_{mixing}) < 0 \qquad (1)$$

The entropy change, ΔS_{mixing}, is the sum of positive and negative changes. The gain in the entropy comes from the break-up of the crystal lattice and the deformations in the polymer structure. Localized ordering of the polymer host by ions can give a net decrease in entropy. Overall, the dissolution of inorganic salts in the polymer matrix is usually accompanied by a negative change in entropy [4].

The enthalpy change, ΔH_{mixing}, is the result of electrostatic interactions between the cation positive charge and the negative charges on the polymer, or

from partial sharing of a lone electron pair on a coordinating atom in the polymer. This also means, for most polymer/salt complexes, cations should bind to the polymer chain instead of other ions. Also, to freely move in the polymer matrix, anions should have minimal interactions with the polymer and the cations [4]. To satisfy all these requirements, e.g., weak anion-cation interaction and strong cation-polymer bonding, a salt with a small univalent cation and a large anion is needed, such as lithium iodide (LiI) as used in our work. Recently ionic liquids have also been used for the design of polymer electrolytes.

The solubility of cations in the polymer is determined by cation – polymer interactions, which can be predicted by the hard/soft acid base (HSAB) principle [3, 4]. The HSAB principle was formulated by Pearson as a means to explain and predict the solubility of complexes formed between Lewis acids and bases. A "hard" acid consists of smaller and non polarizable cations, e.g. alkali ions, while a "soft" acid has larger and easily distorted cations, e.g. Hg^{2+}. A "hard" base has non-polarizable ligands with high electronegativity, e.g. ether oxygen, while a "soft" base has ligands with more polarizable groups, e.g. thio group in thioether. The HSAB principle states that matching hard acid with hard bases or soft acid with soft bases, yields the strongest interactions, or the strongest solvation. Therefore for PEO polymers with hard bases, the best candidates for cations are non-polarizable small cations, e.g. Li^+, Na^+.

To dissolve ions in less polar solvents, such as polyether, a large anion

with delocalized charge is required. The following order predicts the most appropriate anions for polyether-based polymer electrolytes [3, 4]:

$$F^- << Cl^- < I^- \sim SCN^- < ClO_4^- \sim CF_3SO_3^- < BF_4^- \sim AsF_6^-$$

Large and polarizable monatomic anions, e.g. I, are very easily dissolved in polyether-based polymer electrolytes.

An important aspect of ion - polymer interactions is the chelate effect [23]. It occurs when simple solvent molecules coordinated to a central ion are replaced by multidentate ligands, i.e. molecules that can form more than one bond with the central ion. An example of such a process is the exchange of four water molecules coordinated to Li^+ ion for a single PEO chain that can provide four ether oxygens. The total reaction, which consists of four steps, can be written as:

$$[Li(H_2O)_4]^+ + PEO \Leftrightarrow [Li(PEO)]^+ + 4H_2O$$

The disorder of the whole system is increased because there are two species on the left side of the equation and five species on the right side. This leads to a large positive entropy and explains why, in general, chelate complexes are very stable. The example reaction is also very relevant to our study as it determines how Li ions will be distributed between water and polymer, and how efficiently they will move through the solution. The total equilibrium concentrations of lithium complexes will depend on both the favorable enthalpy of Li-water interactions and increased entropy associated with binding to PEO chains.

2.4 Conductivity Mechanism

Conductivity is often used to characterize the performance of polymer electrolytes and an approximate value of $10^{-5}Scm^{-1}$ has been adopted as a minimal requirement for practical applications [4]. Our understanding of the ion transport mechanism is complicated and not completely clear because many of the polymer electrolytes studied have more than one phase. However, it has been shown that the amorphous phase is responsible for the ionic conductivity [3, 4]. At high temperatures, the crystalline phase can dissolve in the amorphous phase which has a higher concentration of charge carriers, thus increasing ionic conductivity [3, 4]. Higher ionic conductivity means that more charge can be transported through the polymer electrolyte per unit time. In other words, it represents one important performance measure for a polymer battery. As a result of the motion of polymer chains, cations are able to move between co-ordination sites, (such as oxygen atoms in the PEO polymer chain), either on one chain or between neighboring chains, called intrachain hopping and interchain hopping respectively shown in Figure 5 [3]. Moreover, considering ion association from the ion-ion interactions between ions, there are other types of hopping mechanisms involving an ion cluster, as shown in figure 6. The extent of these movements is dependent on the concentration of ions in the polymer host. It is assumed that interchain hopping brings about high ionic conductivity [3]. To

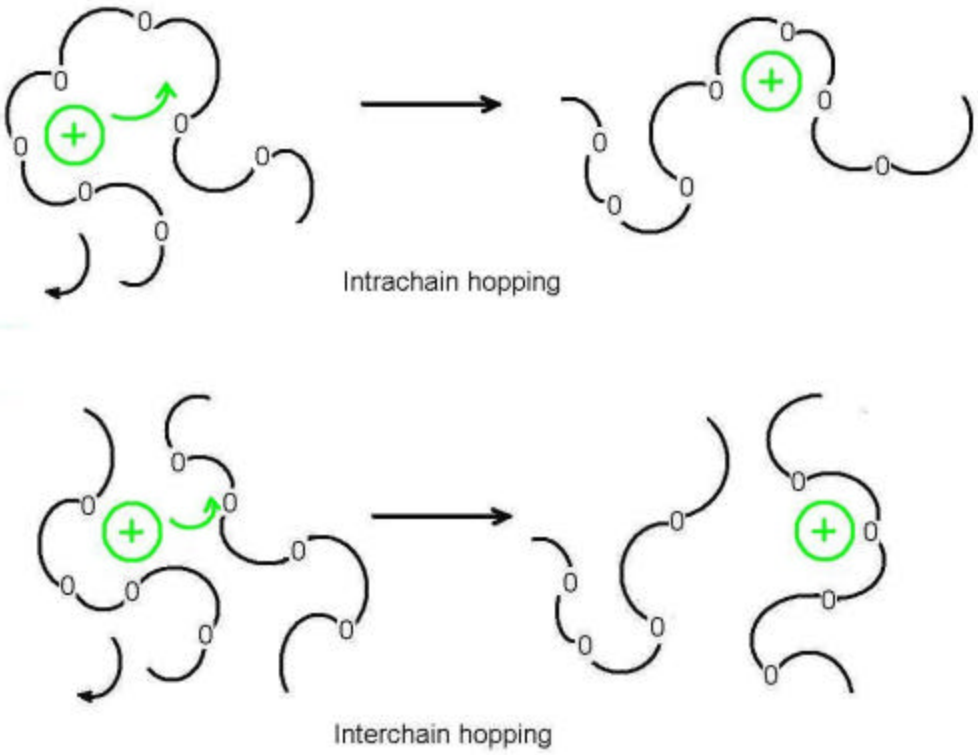

Figure 5: Cation motion in a polymer electrolyte assisted by polymer chains only [3].

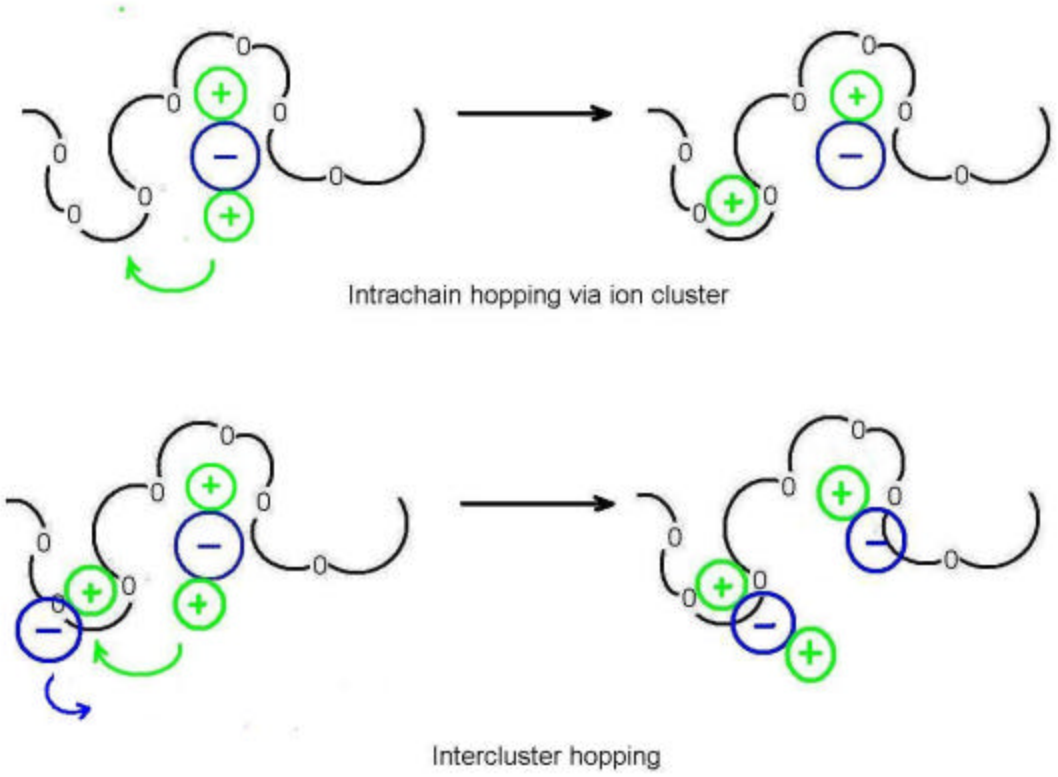

Figure 6: Cations motion in a polymer electrolyte facilitated by the ionic cluster [3]

date, the conductivity mechanism in polymer electrolytes is still not fully understood. In this work we try to gain insight into the mechanisms of ion conduction in systems containing water molecules. As will be discussed in later chapters, water has a dramatic influence on the ions (Li^+) transport behavior, by breaking pairs of counter ions and separating the polymer chains, making interchain hopping and ion cluster facilitated mechanisms less likely.

2.5 Effect of humidity on SPEs

Previous experimental and theoretical research on PEO/salt electrolytes [9, 10, 12, 24-26] have yielded a fundamental understanding of several aspects of ion-transport phenomena, such as ion association at high temperature or high ion concentration, the obstruction of ion movement due to crystalline phases of PEO, etc. Furthermore, experiments have revealed many attractive properties are possessed by ternary mixtures of SPEs in aqueous solution, such as a changed cation environment and increased ionic conductivity after adding water [11, 21, 27]. However, there is still much to be understood. Previous molecular dynamics simulations have mostly focused on PEO/salt binary solutions and proven that cations are transported through the amorphous phase of PEO polymer [8-10];

In 1998, Hashmi made use of X-ray diffraction (XRD) [11], differential

thermal analysis (DTA) and thermo gravimetric analysis (TGA) to study the effect of humidity on thermal behavior and microstructure of solid polymer electrolytes. The disappearance of XRD peaks after exposure to a humid environment indicated a large change in lamellar microstructure of the PEO matrix. Hashmi also noticed that the electrical conductivity of the polymer complexes increases with increasing relative humidity [11]. Similarly increases in conductivity were also found by Lauenstein and coworkers [27] via AC impedance spectroscopy experiments, explained by the conjecture that the absorbed water molecules are bound to the ions, especially the cations formerly bonded to polymer oxygen [27]. Another explanation given by Wendsjo for increased conductivity of polymer complexes is that the coordination between oxygen of PEO and the cations is weakened due to the presence of water, so that it produces more free mobile ions [28].

These conjectures about the change of the cation environment being influenced by water have been supported via neutron scattering experiments by Annis and coworkers [21]. Neutron scattering experiments clearly show that adding PEO into lithium aqueous solutions does not change the hydration structure of cations significantly. Since water has a stronger ability to solvate ions than PEO, more cations are found near the water oxygens instead of the ether oxygens. Another interesting finding is that while both PEO and salts are individually highly soluble in water at moderate temperature, they become less

soluble in the ternary mixture. PEO polymer chains have a lower critical solution temperature (LCST) at high molecular weight, which means solubility of PEO is decreased by increasing temperature. This phenomenon can be explained by the fact that the bonds between water hydrogen and ether oxygen, the main molecular mechanism permitting dissolution of PEO chains in water, are weakened with increasing temperature. Cations can disrupt these bonds by being coupled with water molecules; therefore the presence of cations can have the same effect as increasing temperature on PEO aqueous solutions [29-31].

2.6 Experimental methods

In the remaining part of this chapter we describe currently available experimental methods and the connection between experimental data and our simulation results. Experimental methods are the most fundamental scientific tool and the ultimate test for any theory. While the interpretation of the data produced is not always unequivocal, as in the case of some scattering experiments, they provide bounds to predictions for computer simulations [5, 20]. Many of the most valuable results for comparison with simulations are provided by neutron scattering and the measurement of conductivity.

2.6.1 Neutron scattering experiments

Figure 7 shows a representation of a typical neutron scattering experiment, in which q is the scattering angle and $\vec{k}$ is the wave vector of the neutron. Momentum transfer $\vec{Q}$ can be regarded as the difference between the incident and scattered wave vectors ($\vec{k}_1$ and $\vec{k}_2$ respectively [32]),

$$\vec{Q} = \vec{k}_1 - \vec{k}_2 \tag{2}$$

Neutron scattering experiments measure the number of neutrons scattered per unit time into solid angle Ω and energy transfer w in terms of the double differential cross-section, given by [32-34]:

$$\frac{\partial^2 s}{\partial \Omega \partial w} = \frac{k_2}{k_1} \sum_{i,j} b_i b_j \frac{1}{2p} \int_{-\infty}^{+\infty} e^{iwt} \left\langle e^{-i\vec{Q}\bullet\vec{r}_i(0)} e^{i\vec{Q}\bullet\vec{r}_j(t)} \right\rangle dt \tag{3}$$

where b_i denotes the neutron scattering length of atom i, $\vec{r}_i$ denotes the position of atom i at time t and k_i is the absolute value of the wave vector $\vec{k}_i$ of neutrons. The bracket $\langle\ \rangle$ denotes thermal averages.

Considering the different scattering length for atoms of the same type and replacing the scattering lengths by the average $\langle b \rangle$ and variance $\sqrt{\langle b^2 \rangle - \langle b \rangle^2}$, equation (2) may be divided into 2 incoherent and coherent parts [32-34],

$$\frac{\partial^2 s}{\partial \Omega \partial w} = \left(\frac{\partial^2 s}{\partial \Omega \partial w} \right)_{incoherent} + \left(\frac{\partial^2 s}{\partial \Omega \partial w} \right)_{coherent} \tag{4}$$

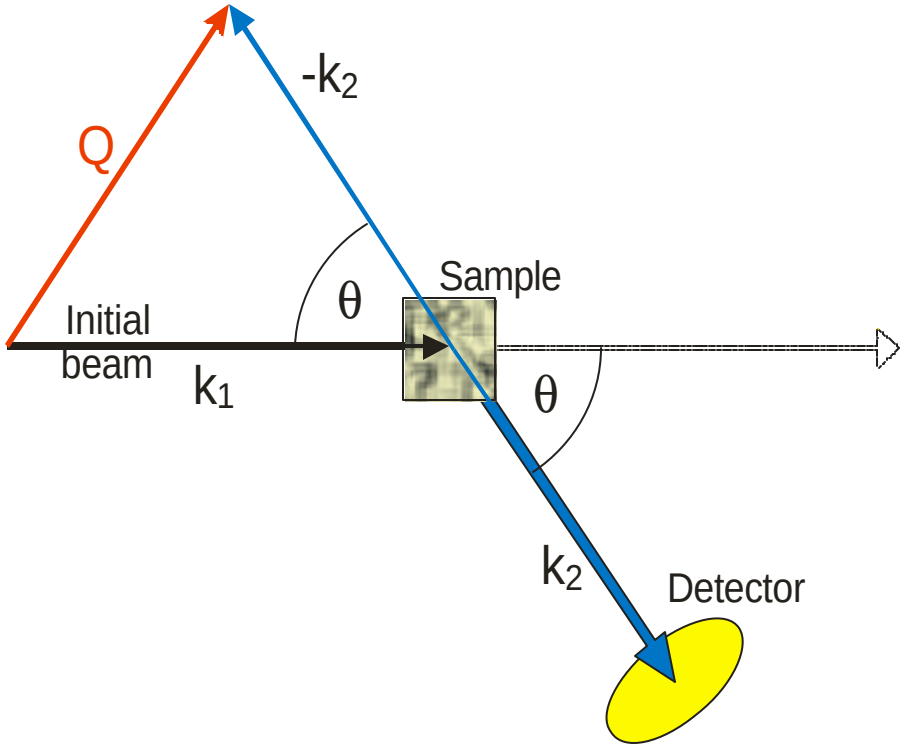

Figure 7: Schematic of a neutron scattering experiment [32].

$$\left(\frac{\partial^2 s}{\partial\Omega\partial w}\right)_{incoherent} = \frac{k_2}{k_1}\underbrace{\sum_{i,j}\left\{\left\langle b^2\right\rangle - \left\langle b\right\rangle^2\right\}\frac{1}{2p}\int_{-\infty}^{+\infty} e^{iwt}\left\langle e^{-i\vec{Q}\bullet\vec{r}_i(0)}e^{i\vec{Q}\bullet\vec{r}_j(t)}\right\rangle dt}_{S_{incoherent}(\vec{Q},w)} \tag{5}$$

$$\left(\frac{\partial^2 s}{\partial\Omega\partial w}\right)_{coherent} = \frac{k_2}{k_1}\underbrace{\sum_{i,j}\left\langle b^2\right\rangle\frac{1}{2p}\int_{-\infty}^{+\infty} e^{iwt}\left\langle e^{-i\vec{Q}\bullet\vec{r}_i(0)}e^{i\vec{Q}\bullet\vec{r}_j(t)}\right\rangle dt}_{S_{coherent}(\vec{Q},w)} \tag{6}$$

Here, $S_{incoherent}(\vec{Q},w)$ and $S_{coherent}(\vec{Q},w)$ are the so-called incoherent and coherent neutron scattering factors, respectively. Coherent neutron scattering factors describe the relative motions of atoms, and they are the most readily available experimental data, in the format of static structure factor, $S(Q)$ [32-34],

$$S(Q) = \int_{-\infty}^{\infty} S_c(Q,w)dw \tag{7}$$

where Q is the magnitude of $\vec{Q}$, i.e., $Q = \left|\vec{Q}\right|$. For multi-component systems, the static structure factor is usually separated into partial structure factors, $S(Q)$, by

$$S(Q) - 1 = \frac{\sum_i\sum_j c_i c_j \left\langle b_i\right\rangle\left\langle b_j\right\rangle\left(S_{ij}(Q) - 1\right)}{\sum_i c_i\left\langle b_i^2\right\rangle} \tag{8}$$

where parameters c_i and c_j are the atom fractions of atom type i and j respectively [5, 35],

We can then compute the partial pair distribution functions $g_{ij}(r)$ by Fourier transform,

$$g_{ij}(r)-1=\frac{1}{2p^{2}r}\int_{0}^{\infty}Q^{2}\left(S_{ij}(Q)-1\right)\frac{\sin Qr}{Qr}dQ \qquad (9).$$

where r is the number density. Hence, in principal, if the individual $S(Q)$ can be extracted from the neutron scattering data, the $g_{ij}(r)$ can be obtained for comparison to its molecular simulation counterpart. In practice, however, $S(Q)$ is not known for all Q, which can lead to difficulty in obtaining $g_{ij}(r)$ from experimental $S(Q)$.

To determine individual $S(Q)$, various atoms are systematically substituted with isotopes (e.g., replacing hydrogen atoms by deuterium atoms thus changing the scattering length while leaving the $g_{ij}(r)$ unchanged). From the $S(Q)$ for varying degrees of isotropic substitution, the individual $g_{ij}(r)$ can be extracted. This technique is called neutron diffraction by isotropic substitution (NDIS) [33, 34, 36] and has been a standard technique for determing atomic-level distribution functions for many decades.

2.6.2 Measurement and calculation of cunductivity

Beside neutron scattering experiments which is able to detect the structural properties of polymer electrolytes, nuclear magnetic resonance (NMR) methodologies can be used to determine information about mobility mechanisms in polymer electrolytes by measuring the spin-lattice relaxation time T_1 and the linewidths (Δv) as a function of temperature for ^{1}H, ^{13}C, and

^{7}Li nuclei [37]. To connect these experiments with our simulation, we used the following equations to calculate the diffusion coefficient and corresponding conductivity, the most important quantities that can be used to analyze ions transport behavior in polymer host and compared to their experimental counterpart.

Considering correlated motions of anions and cations, we define a collective ion diffusion coefficient D_{coll} by [10]

$$D_{coll} = \lim_{t\to\infty} \frac{1}{N_{cations} + N_{anions}} \sum_{i=1}^{N_{cations}} \sum_{j=1}^{N_{anions}} z_i z_j \frac{\left\langle \mathbf{R}_i(t) \bullet \mathbf{R}_j(t) \right\rangle}{6t} \tag{10}$$

where $N_{cations}$ and N_{anions} are the number of cations and anions of the system, i and j represent cations and anions, respectively. Z_i is the charge of the ion i in units of the absolute value of electronic charge, e. $\mathbf{R}_i(t)$ is the vector displacement of the center of mass of species i during time t. The corresponding conductivity of the system, l, is calculated as [10]

$$l = \frac{e^2 \left(N_{cations} + N_{anions}\right)}{V k_B T} D_{coll} \tag{11}$$

where V is the volume of the simulation box. T is the system temperature, and k_B is the Boltzmann constant [10]. Replacing the total number of ions by the number of lithium ions in the system, we can also calculate the self-diffusion coefficient of species i, D_{Li}^{self}, to obtain a picture of how the individual ions move [10],

$$D_{Li}^{self} = \lim_{t\to\infty} \frac{\left\langle \mathbf{R}_i^2(t) \right\rangle}{6t}, \tag{12}$$

the corresponding conductivity of lithium ions can also defined as:

$$l_{Li} = \frac{e^2 N_{Li}}{V k_B T} D_{Li}^{self} \tag{13}$$

CHAPTER III

3 MOLECULAR DYNAMICS SIMULATIONS

It would be very time-consuming, expensive and perhaps impossible to carry out traditional experiments (including NDIS experiments) to explore all of the properties of polymer electrolytes. However, the exponential growth in computational power has enabled a corresponding growth in molecular modeling, the theoretical methods and computational techniques used to model the behavior of complex molecular systems at the atomic and molecular levels. Molecular modeling has been proven to be a promising tool to investigate systems, particularly in situations where carrying out experiments may be costly or impossible. Molecular dynamics simulation has been used to study molecular systems in the fields of computational chemistry, material science, and biology [38-40].

For a successful simulation, an accurate forcefield which describes the inter- and intra-molecular interactions among the atoms and molecules of the simulated system is needed. For the systems defined here, we need to model the interactions between PEO, inorganic salts, and water, in addition to the relevant

intramolecular interactions. This section covers the development of the forcefields for PEO polymer and PEO/salts complexes, and recent experimental findings regarding the effect of humidity on the polymer electrolytes, which form the motivation for our work.

3.1 Molecular dynamics simulation

Molecular dynamics (MD) simulation is a method for generating atomic trajectories by integration of the equations of motion. For example, in MD typically we numerically solve Newton's law, described by the following equations of motion [38]:

$$\mathbf{f_i} = m_i \mathbf{a_i} = m_i \frac{d^2 \mathbf{r_i}}{dt^2} \tag{14}$$

where $\mathbf{f}_i$ is the force on atom i due to interactions with all other atoms in the system, $\mathbf{a}_i$ is acceleration, and m_i is atomic mass.

In a molecular dynamics simulation, atoms, including both nuclei and electrons together, are typically described as spheres with van der Waals interactions and point charges located at the center. The force $\mathbf{f}_i$ is obtained as the negative gradient of potential energy U with respect to $\mathbf{r}_i$,

$$\mathbf{f_i} = -\nabla_{\mathbf{r_i}} U \tag{15}$$

Therefore, by numerical integration, using a method such as Verlet leapfrog or predictor-corrector [38], it is possible to calculate the positions and velocities

($\mathbf{v_i}$) of all particles in the system and generate a trajectory (visualizable as a movie) showing how the atoms move in the system over the time integrated. In the work presented, we used the relatively simple but sufficiently accurate and time-reversible Verlet leapfrog integrator. In this method, the position $\mathbf{r}_i$ of atom i in time $t + \Delta t$, where Δt is the integration time step, is calculated as

$$\mathbf{r}_i(t + \Delta t) = \mathbf{r}_i(t) + \Delta t \mathbf{v}_i(t + \tfrac{1}{2}\Delta t). \quad (16)$$

Here $\mathbf{v_i}(t + \frac{1}{2}\Delta t)$ is the velocity of atom i half time step between two subsequent time points used to calculate positions $\mathbf{r}_i$. The velocity is calculated from the velocity at $t - \frac{1}{2}\Delta t$ and forces $\mathbf{f}_i$ acting on atom i at time t.

$$\mathbf{v_i}(t + \tfrac{1}{2}\Delta t) = \mathbf{v_i}(t - \tfrac{1}{2}\Delta t) + \Delta t \frac{\mathbf{f_i}}{m_i} \quad (17)$$

This alternating calculation of positions and velocities jumps inspired the name 'leapfrog'. The velocity at time t can be calculated as the average of the velocities at times $t + \frac{1}{2}\Delta t$ and $t - \frac{1}{2}\Delta t$:

$$\mathbf{v}_i(t) = \frac{1}{2}\left[\mathbf{v}_i(t + \tfrac{1}{2}\Delta t) + \mathbf{v}_i(t - \tfrac{1}{2}\Delta t)\right] \quad (18)$$

In molecular dynamics simulations, the system temperature and pressure can be kept at or around preset values by using several types of thermostats and barostats [38]. These employ different approaches, such as adding artificial degrees of freedom, imposing constraints on kinetic energy, or modifying the equations of motion by adding special 'friction' terms [38]. In this work, we use the method devised by Nose and Hoover [41, 42] in which temperature and

pressure are associated with new artificial degrees of freedom. Their motion, representing temperature and pressure changes, is then calculated using equations of motion similar to those for atomic trajectories.

Most structural information on fluid systems is obtained in the form of the pair correlation functions, which provide information on the conditional probability of finding a pair of atoms at a given mutual separation. In simulations, it can be measured by collecting histogram, $H(r-dr, r+dr)$ of particle separations between $r-dr$ and $r+dr$ and normalizing it according to [38]:

$$g(r) = \frac{V}{4pr^2N^2} * H(r-dr, r+dr) \qquad (19)$$

where V is the system volume and N is the number of atoms.

3.2 Forcefields for MD simulations

In the context of molecular modeling, a forcefield means the energy functions and parameter sets used to calculate the potential energy of a system. The energy functions and parameter sets are either derived from quantum chemistry calculations or empirically from experimental data. Typically, classical forcefields (described here) employ two-body pairwise additive potentials and ignore multi-body dispersion and many-body polarization effects. The basic functional form of a classical forcefield can be regarded as the sum of

nonbonded interactions, also called intermolecular interactions, and intra-molecular interactions (bond stretch, valence angles and dihedral angles):

$$E = \sum_{i \neq j} E_{ij}{}^{NB}(r) + \sum_{ij} E_{ij}{}^{s}(r) + \sum_{ijk} E_{ijk}{}^{b}(q) + \sum_{ijkl} E_{ijkl}{}^{t}(\Phi) \quad . \tag{20}$$

where r is the distance between atom centers, $E_{ij}{}^{NB}(r)$ is the nonbonded energy associated between atom i and j, $E_{ij}{}^{s}(r)$ is the covalent bond stretching energy between atom pair i and j, $E_{ijk}{}^{b}(q)$ is the bond-angle bending energy that depends on the angle q formed by atoms i, j and k, and $E_{ijkl}{}^{t}(\Phi)$ is the torsional energy arising from rotation around the dihedral angle Φ defined by atoms i, j, k and l. Nonbonded interactions $E_{ij}^{NB}(r)$, the interactions between atoms in different molecules or in the same molecules separated by two or more atoms, are composed of electrostatic interactions and van der Waals interactions as given by:

$$E_{ij}{}^{NB}(r) = E_{ij}^{elec}(r) + E_{ij}^{vdw}(r) \tag{21}$$

The summations run over all interactions of each type present in each molecule and between molecules. The bond-stretch, bond-angle and torsional-angle terms have many forms. In the vast majority of forcefields used in molecular dynamics simulations, bond breaking is not possible; this is also the case for the forcefields used in this work. The electrostatic energy, E_{ij}^{elec}, also called the Coulombic energy, is directly related to atomic charges by Coulombs law,

$$E_{ij}^{elec}(r) = \frac{1}{4pe_0}\frac{q_i q_j}{r} \tag{22}$$

where q_i, q_j are the charges on atoms i and j, and e_0 is the permittivity of free space. There are many forms used to describe the van der Waals energy. The two most popularly used are the Lennard- Jones (LJ) potential, [43]

$$U(r) = \left(\frac{A}{r^{12}}\right) - \left(\frac{B}{r^6}\right) = 4e\left[\left(\frac{s}{r}\right)^{12} - \left(\frac{s}{r}\right)^6\right] \tag{23}$$

where $A = 4es^{12}$ and $B = 4es^6$ and the Buckingham potential,

$$U(r) = A' \exp(-B'r) - \frac{C'}{r^6} \tag{24}$$

In equation (23) and (24), A, B, e, s, A', B' and C' are constants fitted to *ab initio* and/or experimental data. The parameters A' and B' determine the short range repulsive interaction, C' is the dispersion parameter. The parameters e and s have the significance of being the depth and zero point of the potential. Both the LJ and Buckingham potential include the long-range London dispersion term.

Such classical forcefields are used widely in the molecular dynamics simulations of polymer electrolytes, but recent molecular dynamics simulations by Smith and coworkers have shown that polarization effects can play a very important role for these systems and should not be ignored [31]. In the following section, we describe the definition of polarization, its influence on the environment of lithium in a PEO polymer, and possible methods for including it in a forcefield.

3.3 Polarizability and its modeling

Large-scale quantum chemical calculations have shown that polarizability, also called electrical induction-charge redistribution within a molecule due to an external electric field, is very important for determining the structural and dynamic properties of certain molecular clusters. It can play a key role in some phenomena, such as ion solubility and dielectric properties [44]. For instance, as pointed out by previous research, the induced dipole of liquid water can be as large as 50% of the permanent dipole of liquid water [44]. The Cummings group is at the forefront developing highly accurate polarizable models for water [45-48].

In previously reported molecular simulations [14, 31], the non-bonded potentials needed for PEO polymers were pairwise additive, and used artificially large partial charges to compensate for the missing polarizability at the atomic level [49]. These pair-wise additive potentials were of the form

$$E_{ij}^{NB}(r) = A_{ij}\exp(-rB_{ij}) - C_{ij}r^{-6} + \frac{1}{4\pi\varepsilon_0}\frac{q_i q_j}{r} \qquad (25)$$

That is, they combine the Buckingham model for van der Waals forces with a point-charge model for electrostatics [14]. However, this nonpolarizable forcefield has its limitations, as proven by Smith and coworkers who compared three forcefields differing in their treatment of the polarizability, thus probing the importance of polarization effect on the properties of solid PEO/LiI

electrolytes in their simulations and hence also real systems [31]. We have performed similar simulations to test our simulation methodology, the results of which will be given in section 4.3

The incorporation of the polarization effects into molecular simulations is typically done in one of three ways. The simplest way is to include the average effective induced dipole moment into the permanent dipole moment of a molecule. Examples are the simple point charge SPC and transferable intermolecular potential TIP4P models for water which have 20% or larger permanent dipole than that of a water dipole in the gas phase [50]. However this approach is limited to the density and temperature conditions where the effective dipole is fitted. For non-polarizable models of water with fixed enhanced dipole moment, the forcefield cannot be expected to be accurate except at ambient conditions where the effective dipole moment is fitted. The most accurate but computationally most expensive method to study dynamics is to use molecular dynamics with forces calculated on the *ab initio* quantum mechanical (QM) methods, such as Car-Parrinello Molecular Dynamics (CPMD) [51]. However, in contrast to other models, CPMD is at least five orders of magnitudes more computationally expensive even for small (32 molecules) systems; moreover, the calculation time grows as N^3, where N is the total number of atoms in the system. The third, intermediate and more cost-effective way is to introduce explicit polarization into classical molecular dynamic

simulations, as for example, in the Gaussian charge polarizable model (GCPM) developed in the Cummings group [52], the most successful model for water in the published literature.

When considering including the effect of polarizability into a forcefield, several options and limitations must be considered [53]:

1) Most polarizable forcefields are parameterized based on both the gas phase and condensed phase. This differs from a non-polarizable model, in which the effective dipole moments are fitted to reproduce the condensed phase data only [53].

2) The atomic polarizability of an atom i, $\mathbf{a}_i$, is in principle a tensor quantity [53],

$$\mathbf{a}_i = \begin{pmatrix} \mathbf{a}_{xx} & \mathbf{a}_{xy} & \mathbf{a}_{xz} \\ \mathbf{a}_{yx} & \mathbf{a}_{yy} & \mathbf{a}_{yz} \\ \mathbf{a}_{zx} & \mathbf{a}_{zy} & \mathbf{a}_{zz} \end{pmatrix} \tag{26}$$

and precise values of all components are not easy to determine. For computational simplicity, and when warranted by physical insight, the isotropic polarizability, i.e.,

$$\mathbf{a}_i = a_i \begin{bmatrix} 1 & 0 & 0 \\ 0 & 1 & 0 \\ 0 & 0 & 1 \end{bmatrix} \tag{27}$$

is frequently assumed, as in the simulations reported here.

3) Putting inducible dipoles on all atoms of the system is computationally expensive, and can lead to polarization catastrophe, which occurs when two

inducible dipoles are spatially too close to each other [54]. To simplify the simulation and avoid this problem, polarization centers are often put only on selected atoms or groups of atoms.

There are three main methods to represent induced dipoles in the simulated system. These are:

A) The point-polarizable dipole (PPD) model, in which a point dipole characterized by polarizability a_i, is located at sites r_i in a molecule [53].

B) The fluctuating-charge (FQ) model, in which atomic point charges q_i change in response to the changes in a local electric field [53].

C) The shell model, in which a polarizable atom is represented by a core and shell unit that is connected through a harmonic spring [55].

For the point-polarizable dipole (PPD) model, the total electrostatic energy U_{el} of a system composed of static point charges , q_i, and induced dipoles, $\boldsymbol{\mu}_i$, is the sum of the energies coming from charge-charge, charge-dipole, and dipole-dipole interactions. The electric field, E_i at the location of an interaction site i (point charge or point dipole) can be decomposed into a part due to point charges, E_i^0, and a part due to dipoles [53, 56]:

$$\mathbf{E}_i = \mathbf{E}_i^0 + \sum_{j=1,\, j\neq i} \mathbf{T}_{ij} \bullet \boldsymbol{\mu}_j \qquad (28)$$

where,

$$\mathbf{E}_i^0 = \sum_{j=1, j\neq i} \frac{1}{4\pi e_0} \frac{q_j \mathbf{r}_{ij}}{r_{ij}^3} \tag{29}$$

with $\mathbf{r}_{ij}$ distance vector from i to j, and in the second term,

$$\mathbf{T}_{ij} = \frac{1}{4\pi e_0} \frac{1}{r_{ij}^3} \left(\frac{3\mathbf{r}_{ij}\mathbf{r}_{ij}}{r_{ij}^2} - 1 \right) \tag{30}$$

T_{ij} is the dipole-dipole interaction tensor. Dipole moments $\boldsymbol{\mu}_i$ characterized by atomic polarizability a_i are induced by electric field E_i according to

$$\boldsymbol{\mu}_i = a_i \mathbf{E}_i$$

where we have assumed isotropic (scalar) polarizability. The total electrostatic energy can be then decomposed as [50, 52, 53]:

$$U_{el} = U_{qq} + U_{qp} + U_{pp} + U_{self} \quad , \tag{31}$$

where U_{qq} is the energy of pairs of interacting point charges

$$U_{qq} = \frac{1}{2} \sum_{i}^{N} \sum_{\substack{j=1 \\ i\neq j}}^{N} \frac{1}{4\pi e_0} \frac{q_i q_j}{r_{ij}} \quad , \tag{32}$$

U_{qp} is the energy of dipoles interacting with the electric field produced by point charges

$$U_{qp} = -\sum_{i=1}^{N} \boldsymbol{\mu}_i \mathbf{E}_i^0 \quad , \tag{33}$$

U_{pp} is the energy of interacting dipole pairs

$$U_{pp} = -\frac{1}{2} \sum_{i=1}^{N} \sum_{\substack{j=1 \\ i\neq j}}^{N} \boldsymbol{\mu}_i \bullet \mathbf{T}_{ij} \bullet \boldsymbol{\mu}_j \quad , \tag{34}$$

and U_{self} is the energy needed to separate the opposite charges of a dipole,

$$U_{self} = \sum_{i=1}^{N} \frac{m_i^{\,2}}{2a_i} \quad . \tag{35}$$

For many practical applications, atomic polarizabilities are preferably modeled by the shell model, which can be easily implemented in a computer simulation because charge-charge and bonding interactions already exist in the forcefield. Since our simulation software (DL_POLY) [57] does not include the option of point dipoles or fluctuating charges, we used the shell model to introduce polarization effects into our forcefields. In order that the equations of motion for the core-shell unit can be integrated, a small fraction of the total mass is assigned to the shell, in the so-called dynamic shell model. The core and shell are connected by a harmonic spring with a spring constant k determined by atom's polarizability a [55]:

$$a = q_s^2 / k \tag{36}$$

where q_s is the charge of the shell. The total atomic charge is then recovered as the sum of the charge of core, q_c and shell charges q_s. Core-shell units could be thought of similar to a diatomic molecule with a harmonic bond, where there is no Coulomb interaction between the core and shell of the same atom, and at larger distances they interact as polarizable point dipoles. Short range (VDW) interactions are usually assigned to shells alone. The polarization energy can be written as [55]:

$$U_{ij}^{\,pol}(r) = \frac{1}{2} k r^2, \tag{37}$$

where r is the distance between a core and its shell. Figure 8 is an illustration of shell model.

3.4 Parameterization of empirical and *ab initio* forcefields

Generally, there are two ways to develop a forcefield: one is empirical, based on experimental data and the other is theoretical, based on *ab initio* calculations. Many forcefields are developed using a combination of these two methods. However, the majority of current forcefields are semi-empirical. As the name suggests, semi-empirical forcefields are optimized to reproduce experimental data, either microscopic data, such as average bond lengths or dipole moments, or thermodynamic data, such as density or heat of vaporization. However, since a given forcefield is optimized by fitting to a limited range of experimental data, the simulations may not be able to reproduce other properties of the system, or predict properties accurately at state conditions other than those at which the fitting was performed. Therefore, with the goal of better accuracy and generality, forcefield parameters can also be optimized on the basis of *ab initio* quantum chemical calculations. Ideally, one could select the most advanced quantum chemical methods combined with the best basis sets and obtain good predictions of molecular structures and energies. In reality, such calculations can be computationally very expensive, some *ab initio* methods work better for certain

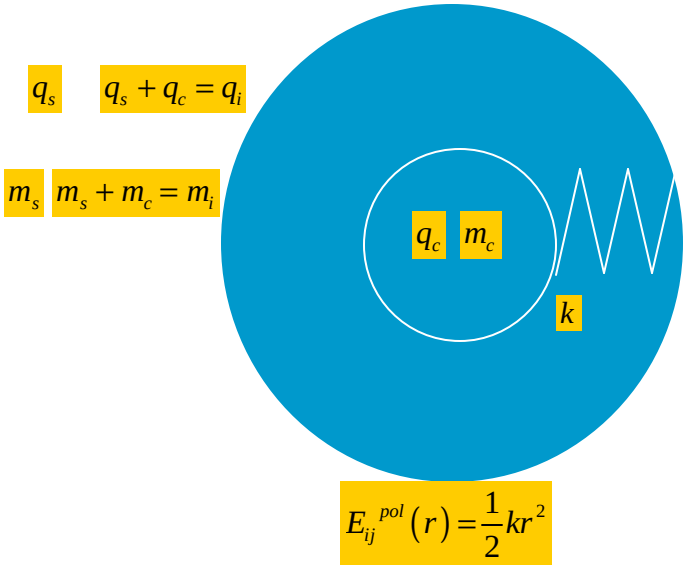

Figure 8: An illustration of the dynamical shell model; m_s and m_c are the masses of the shell and core, respectively; they added up to the mass of the ion, m_i.

properties than for others, and the number of potential parameters is often too

large to be optimized in one step. The procedure is, therefore, usually decomposed into several steps, each done to optimize a selected set of molecular parameters. The structure of molecules and other atom groups can be efficiently predicted using density functional theory (DFT) calculations and the resulting atomic configurations can be subsequently used to calculate energetic properties. Classical forcefields often distinguish between repulsive and attractive van der Walls contributions, with the latter corresponding to dispersion interactions, which are inherently difficult to obtain since they originate in functions with excited states (i.e., they are not obtained purely from ground state properties). As proven by Smith and his coworkers in their work on the development of a many-body forcefield for the PEO polymer [56], the repulsive non-bonded interactions can be relatively easily estimated by using the Hartree-Fock (HF) method, which does not include the effect of dispersion interactions. The parameters of the repulsive part of van der Waals interactions are then optimized by fitting the *ab initio* energies of selected configurations to classical potential functions. The calculation of the dispersion interactions is very difficult and to obtain at least a good estimate, one has to use advanced and computationally expensive quantum chemical methods, such as Moller-Plesset perturbation theory (MPn) or coupled cluster theory (CC), which include higher excitations. Since even these methods do not provide the exact solution of the Schrodinger equation, the results may be further extrapolated and the infinite basis-set limit

estimated [56].

We followed the same method adopted by smith et.al in his work used *ab initio* calculations to determine the parameters of water/PEO potential functions. The detailed description of the procedure is given in Section 5.1 of the results.

3.5 Review of water and PEO forcefields

The development of the intermolecular potential functions for water has been underway for four decades, beginning with the early efforts of Stillinger [58]. Many successful water forcefields have been used in molecular dynamics and Monte Carlo simulations for water and satisfactory results obtained [45-50, 52, 59-60]. In this section we briefly introduce the most popular models of water, some of which were also used in our simulations. The section also covers selected potential models for PEO polymers, ions, and their mixtures.

3.5.1 Extended Simple Point Charge model

For the molecular simulation and Monte Carlo (MC) simulations of water, the most studied polar liquid, effective pair potentials are extensively used, which includes the average many-body interactions into the pair interactions. A typical example is the simple point charge (SPC) model. Due to their lack of explicit polarizabilities and optimization for bulk simulations, these models have larger

dipole moments and second virial coefficients than isolated water molecules. In 1983, Straatsma and co-workers improved the existing SPC water model by inclusion of a self-energy correction, creating a model known as the extended simple point charge model, SPC/E [61].

The SPC/E model can be described as a rigid molecule consisting of one oxygen and two hydrogen atoms, each carrying partial point charges, and the sum of repulsion-dispersion interactions represented by Lennard-Jones potential, between the oxygen atoms. The SPC/E parameters are listed in Table 1.

Table 1: SPC/E water parameters [61]

SPCE	a_O (Å^3)	s (?)	e (kcal/mol)	q_o (**e**)	q_H (**e**)
parameters	0	3.165	0.1554	-0.8476	0.4238

3.5.2 Polarizable SPC model

Sometimes, a proper description of many-body polarizability effects becomes crucial, such as in the presence of high electric fields produced by dissolved ions. These types of situations cannot be correctly described by effective non-polarizable pairwise interactions, which motivated the development of a

wide range of polarizable water models. A direct extension of the above mentioned SPC model is the polarizable SPC model (PSPC), which can directly account for the non-additive contributions due to polarization [62].

Similar to the SPC/E water model, the polarizable SPC model can still be described as the sum of repulsion-dispersion interactions represented by a Lennard-Jones potential with the center located in the oxygen atom, and point-charge Coulombic interactions. However, it also contains contributions from polarization energy, which are introduced through a polarizable center at the location of the oxygen atom [62].

To compensate for the increased attractions due to the induced-dipole interactions, the PSPC model has enhanced repulsions compared to the original SPC model. The parameters are listed in Table 2.

Table 2: PSPC water parameters [62]

PSPC	α_O (Å^3)	σ (Å)	ε (kcal/mol)	q_o (**e**)	q_H (**e**)
parameters	1.44	3.263	0.1294	-0.6690	0.3345

3.5.3 RPOL-Revised Polarizable model

Another model including many-body interactions is the revised polarizable water potential model (RPOL) developed by Dang and coworkers [63]. The form of the forcefield is the same as for PSPC model described above, but it contains three polarizable centers located at the oxygen and both hydrogens, which makes it more complicated to implement in a simulation but consistent with a fully polarizable PEO model described below. As with both previous models, it also contains a Lennard-Jones center located at the oxygen atoms. Good representation of the dynamic properties of pure water and the availability of potential parameters for interactions with Li^+ and I^- ions makes this model particularly attractive for our study [63]. The model parameters are listed in Table 3.

Table 3: RPOL water parameters [63]

RPOL	a_O (Å3)	a_H (Å3)	σ (Å)	ε (Kcal/mol)	q_o (e)	q_H (e)
parameters	0.528	0.17	3.196	0.155	-0.730	0.365

3.5.4 Classical nonpolarizable forcefield for PEO

Smith and coworkers have parameterized nonpolarizable forcefields for simulations of DME and PEO using *ab initio* electronic structure calculations [14, 64]. The total energy of the system, in the form of equation (25), is calculated as the sum of intermolecular interactions, and intra-molecular interactions [14, 64].

As defined before, non-bonded interactions can be decomposed into contributions from dispersion, repulsion and Columbic interactions, and act between atoms in different molecules or atoms in the same molecule separated by two or more atoms [14]. Among the available functional forms, a widely used one is the Buckingham potential function combined with point charge interactions,

$$E_{ij}^{NB}(r) = \underbrace{A_{ij}\exp(-rB_{ij}) - C_{ij}r^{-6}}_{VDW} + \frac{1}{4pe_0}\frac{q_i q_j}{r} \qquad (38)$$

For the van der Waals (VDW) interactions, shown in the above equation, the parameters for the repulsion (A_{ij} and B_{ij}) and dispersion interactions (C_{ij}) for the PEO forcefield were obtained from an empirical forcefield used to calculate crystal structures and energy of a closely related polymer poly-oxymethylene (POM) [14]. The atomic partial charges q_i were parameterized by fitting the dipole moment and satisfying charge neutrality [13, 61].

The intermolecular interaction parameters (k_{ij}^{s}, k_{ijk}^{b} and k_{nijkl}^{t}) and the

geometry parameters (r^0, q^0 and Φ^0) are used to calculate stretching ($E_{ij}^{\ s}$), bending ($E_{ijk}^{\ b}$) and torsion ($E_{ijkl}^{\ t}$) potentials [64],

$$E_{ij}^{\ s}(r) = \frac{1}{2}k_{ij}^{s}(r^0 - r)^2 \tag{39}$$

$$E_{ijk}^{\ b}(q) = \frac{1}{2}k_{ijk}^{b}(q^0 - q)^2 \tag{40}$$

$$E_{ijkl}^{\ t}(\Phi) = -\sum_{n=1}^{3}\frac{1}{2}k_{nijkl}^{t}(n)[(\cos n(\Phi)] \tag{41}$$

and are optimized to fit the geometries and energy of the conformational minima and the rotational energy barriers in DME (the simplest polyether having local conformational properties of PEO polymer) calculated using *ab initio* method [14].

Table 4: Parameters for the nonbonded part of the DME-DME potential [64].

Atom pairs	A(Kcal/mol)	B($Å^{-1}$)	C(Kcal$Å^6$/mol)	$q_i(e)$
C-C	14976	3.090	640.8	-0.066(-0.163)*
O-O	75844	4.063	398.9	-0.256
H-H	2649	3.740	27.4	0.097
C-O	33702	3.577	505.6	
C-H	4320	3.415	138.2	
O-H	14176	3.902	104.5	

* Value in the parentheses is used for the carbon atoms located at the end group (CH_3)

Table 5: Parameters for the bond stretching part of the DME-DME potential [64].

Atom pairs	k_{ij}^{s} (kcal/mol/Å^2)	r^0 (Å)
C-C	618	1.513
C-O	739	1.4
H-H	655	1.09

Table 6: Parameters for the angle bending part of the DME-DME potential [64].

Atom pairs	k_{ijk}^{b} (kcal/mol/ rad)	q^0 (deg)
C-C-H	85.8	109.49
H-C-H	77.0	108.30
O-C-C	119	109.04
O-C-H	112	110.07
C-O-C	149	115.56

Table 7: Parameters for the torsion part of the DME-DME potential [64].

Atom pairs	$k^t_{nijkl}(1)$ (kcal/mol)	$k^t_{nijkl}(2)$ (kcal/mol)	$k^t_{nijkl}(3)$ (kcal/mol)
O-C-C-H	0.00	0.00	-0.28
H-C-C-H	0.00	0.00	-0.28
C-O-C-H	0.00	0.00	-0.81
O-C-C-O	0.05	-2.55	0.00
C-O-C-C	-1.00	-0.70	-0.32
C-C-O-C	-1.00	-0.70	-0.32

3.5.5 Many–body polarizable forcefield for PEO

The forcefields previously described for PEO and oligomers did not include many-body polarizable interactions. Smith and coworkers developed a consistent many-body polarizable forcefield [56, 65]. In this classical forcefield, the total potential energy of the system is again given by equation (41), but includes a polarization term; i.e

$$E^{NB}(r) = \frac{1}{2}\left[\sum_i \sum_j A_{ij} \exp\left(-B_{ij} r_{ij}\right) - \frac{C_{ij}}{r_{rj}^6} + \frac{q_i q_j}{4\pi e_0 r_{ij}}\right] + E^{POL}(r), \qquad (42)$$

where the polarization energy $E^{POL}(r)$, given by equations (28)-(35) is not pairwise additive and is produced when an atom or ion is placed in an electric field. For the many-body forcefield, the electrostatic energy of an atom/ion can not be simply regarded as a function of atomic partial charges. In this case, the

induced dipole moment, which appears at a polarizable atom in an electric field, will also contribute to the electrostatic field around the molecule. Therefore, atomic polarizabilities must be optimized before fitting partial charges. Dykstra's group has published the isotropic atomic polarizabilities of carbon and oxygen of the PEO polymer chain with the hydrogen polarizability included into the polarizabilities of the heavy atoms: $\alpha_{c(sp3)} = 1.874$ Å^3, $\alpha_{-o-} = 0.748$ Å^3 [66]. However, the molecular polarizability of 9.0 Å^3 for DME obtained from the summation of the above atomic polarizabilities is smaller than the quantum chemistry value of 9.1-9.8 ?^{3} for DME, calculated at the B3LYP/aug-cc-pvDZ level [56]. Therefore, Smith and coworkers set atomic polarizabilities by fitting the polarization energy around a molecule using the B3LYP/aug-cc-pvDZ level quantum chemistry calculations. Considering the total polarization energy reproduced by the forcefield using these atomic polarizabilities, and including not only dipole polarization, but also higher-order polarizabilities, it is expected that the forcefield molecular polarizability is slighter higher than the result from quantum chemistry calculation which excludes hyperpolarizabilities. Partial charges are then determined by fitting an electrostatic grid around a DME molecule, using different conformers of DME. Consequently, quantum chemistry calculations are able to predict accurately the van der Waals parameters (dispersion and repulsion) using the procedure outlined in section 3.4. It is relatively easy to get repulsion parameters at HF level quantum

chemistry calculations using the basis set superposition error (BSSE)-correction [56]. However, it is more difficult to get the dispersion energy which requires the larger basis sets and large order methods. To simplify the procedure, the bond and bend force constants were taken from a previously developed nonpolarizable forcefield for PEO, with the equilibrium bond lengths and bending angles optimized to fit the B3LYP/aug-cc-pvDz geometry optimization [56].

3.5.6 PEO/water mixture

Because of their promising applications, many studies have been performed on PEO aqueous solutions [8, 67-70]. However, many experiments, such as calorimetry, scattering, and spectroscopic studies, have produced different, and sometimes contradictory, results about polymer conformations, hydration, and the phase equilibrium behavior in water [8, 71-72]. A clearer understanding may come from molecular simulation studies.

Inaccurate calculation of the PEO/water interactions will result in large differences between simulation and experimental results. The previously validated quantum-chemistry-based forcefield for PEO could be used for calculating polymer-polymer interactions and many water-water potential models (such as SPC/E, PSPC, and RPOL models) are available to calculate the

interaction between water molecules. However, interactions between PEO and water must be determined.

Ether-water interactions consist of electrostatic interactions between carbon, oxygen and hydrogen atoms of the polymer chain and the hydrogen and oxygen atoms of a water molecule. The VDW interactions occur between atoms comprising PEO (C, H, O) and the nonbonded force center of the water model located on the oxygen atom [8]. One way to obtain the cross-interaction parameters of DME-water interactions is by performing molecular dynamics simulations to predict the density of DME-water as a function of composition and temperature and optimize the parameters by comparison to experiments. The alternative is to fit to quantum chemistry values for the binding energy of a DME-water complex as a function of the complex geometry [8, 64]. Figure 9 is an illustration of the polarization effect in DME-water interactions found in the work by Smith et al [64]. The fact that the sum of the binary interactions A, B and C approximately equals the energy of the three-molecule system suggest that the induced interactions - such as the interactions of the water dipole moments with induced dipole moments in DME – may be able to be ignored for PEO/water binary solutions. Therefore, currently simulations of these aqueous binary mixtures use nonpolarizable forcefield.

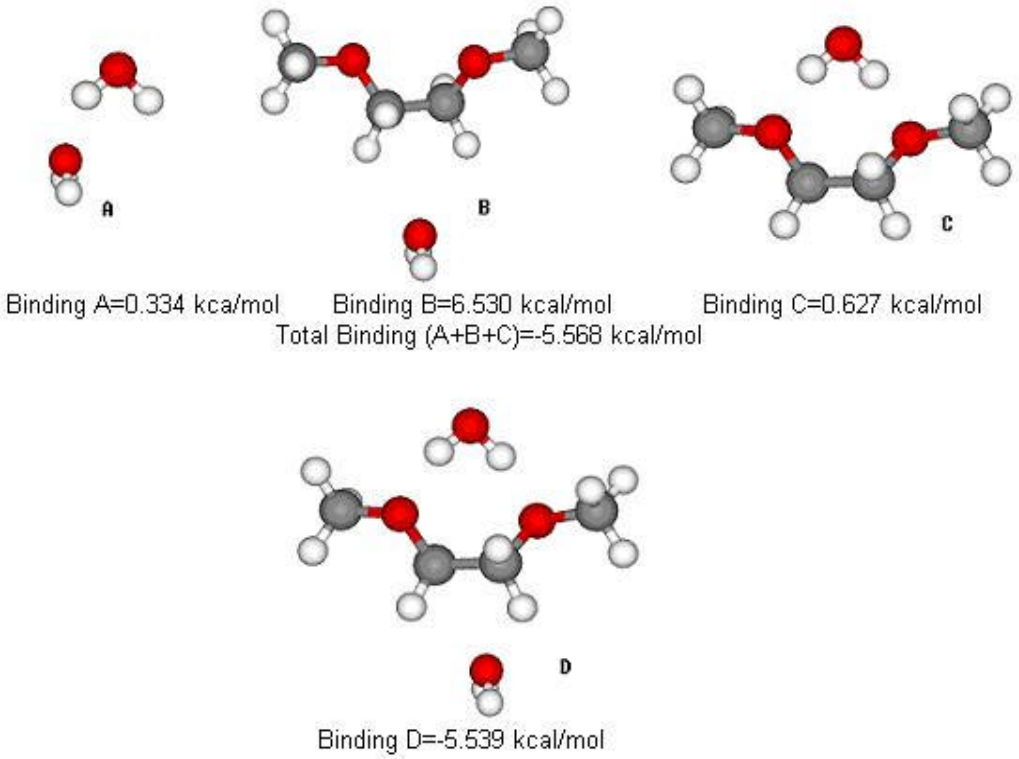

Figure 9: Investigation of the polarization effects in DME-water interactions [8, 64]

3.5.7 PEO/salts

A good polymer electrolyte requires higher ionic conductivity arising from the optimized number and transport behavior of charge carriers, properties which are determined by the interactions of cations, anions and polymer chains. Experimental studies of Raman and infrared spectroscopy of the PEO polymer doped with inorganic salts, such as $LiCF_3SO_3$ and $LiCLO_4$, found that cations will form pairs and aggregates with anions with increasing temperature or increasing ion concentration, resulting in a decreased number of free ions and lower ionic conductivity [9].

Molecular dynamics simulations have supplied important qualitative information about the structure and conductivity mechanism in PEO/salt systems [10, 11, 24, 70]. Because the amorphous phase of PEO is responsible for ion transport, most simulations have been performed at temperatures above the melting point (363K), in the belief that such simulations can give insight into the structure and dynamical properties of PEO/salt systems in the amorphous phase at room temperature. It is believed that the polymer interacts strongly with the cation, forming bonds between cations and ether oxygens, but only weakly with the anions, and that such interactions largely control thermodynamic properties, such as solubility of the salt, and ion mobility [9].

For an accurate molecular simulation in a condensed–phase system, it

would be desirable to include many-body effects, in which the interactions of the ion with any atom of the molecule are actually influenced by its interaction with the other atoms. For polarizable systems, typically the many-body polarizability is the predominant many-body interaction. However many-body effects are computationally expensive to take into account especially when applied to polymer systems. To date, polarizable models accounting for many body effects have been applied to only relatively simple molecules, such as Li^+ in water [73]. As an alterative, effective two-body potential functions accounting for polarizability effects have been frequently employed to approximate the polarization energy for the PEO/salt systems [73],

$$E_{ij}^{pol}(r) = -\frac{1}{4pe_0}[q_i^2 a_j + q_j^2 a_i]/2r^4 + O(r^7) = -D_{ij}/r^4 \qquad (43)$$

where a is atomic polarizability. This approximation is obtained by only considering charge-induced dipole interactions between two atoms, ignoring higher order moments and taking a spherical average [73]. The polarization energy depends on the separation distance and the polarizability of the atoms. Therefore, it can be quite significant even with a neutral atom (charge zero), reflecting the importance of including polarizabilities into the forcefield in highly polarizable systems [69].

CHAPTER IV

4 RESULTS AND DISCUSSIONS

In this chapter, we will describe our simulations and results of the study of structural and dynamic properties of polymer electrolytes. First, we outline our general simulation methodology and approach to the study of polarization effects. In the following sections we discuss the simulations of PEO and its binary mixtures with water and ions, which, in the last step, serve as a basis for the study of the ternary mixture of PEO, LiI, and water. Each of these sections deals first with the forcefield testing or development and is followed by the discussion of structural and dynamic properties.

Our primary goal is to investigate the changes in the structure and dynamics of PEO/salt systems after adding water as the third component. To accomplish this task a good molecular model is needed which includes all important aspects of atomic interactions, such as electrostatic polarization. Previously used effective two-body polarizable forcefields for PEO/salt systems [73] may not be accurate enough for our ternary PEO/salt/water mixtures. It has been shown that polarization does not play an important role in binary PEO/water systems [8] and, therefore, no polarizable forcefield was developed

for these interactions. However, if one wants to simulate a ternary mixture that includes very strong electric fields produced by dissolved ions, one has to incorporate polarization in all components.

To assess the effect of polarization, we ran simulations of PEO and binary mixtures with several forcefields differing in the degree and sophistication to which the polarization was incorporated. The results were compared to available experimental data from neutron scattering and conductivity measurements. Since no force-field was available for water-PEO interactions, we had to develop a new forcefield ourselves and test it against available thermodynamic data, such as density or excess volume for a range of concentrations. We used two approaches to find the optimal model for water–polymer interactions. The first one was based on empirical results and involved rescaling van der Waals parameters so that the simulation predictions correspond to experimental data, and the other was based on quantum chemical calculations of the interactions between one water and one DME molecule, not involving any fitting to empirical data; the second Subsequently, the optimized forcefields were used to simulate and predict properties of the PEO/salt/water ternary mixture that were not available from experiments. Another objective of this study was to elucidate the mechanism of ion conduction in the ternary mixture in relation to the water content.

4.1 Simulation details

All simulated systems consisted of the following species in various concentrations:

a) PEO polymer chains consisting of various numbers of (CH_2-O-CH_2) repeat units or short DME molecules.

b) LiI salt, representing the conducting component of the mixture

c) Water molecules described by the SPC/E, PSPC or RPOL water models

The simulations were carried out in the NVT (canonical) or NPT (isothermal-isobaric) ensembles, by which we mean that the simulated system has a specified density (N/V) and temperature (T) (NVT ensemble) or specified pressure (P) and temperature (NPT) ensemble, to create systems consistent with the corresponding experiments. Temperature and pressure were kept constant using the Nose-Hoover thermostat and barostat [41, 42].

We utilized cubic periodic boundary conditions, by which we mean the central simulation cell (containing 2000-7000 atoms in our simulation) is cubic in shape and is surrounded with exact replicas of itself repeated indefinitely. The minimum-image convention is adopted to insure that each atom interacts only with the nearest atom or image in the periodic array [38].

Because chemical bonds typically vibrate at very high frequencies, which makes the integration of equations of motion very time-consuming (requiring a

very small timestep, usually 1-4 fs), all chemical bonds were constrained to their equilibrium lengths by the SHAKE algorithm [74], allowing the use of a considerably larger time step. The Ewald summation method was employed to treat long-range Coulumbic interactions [38]. All simulations were performed using DL_POLY_2 [57], a computational molecular dynamics simulation software package, developed at Daresbury Laboratory by Smith and Forester. DL_POLY was modified to include the functional form of the torsional potentials used in this work. The dynamic shell model was used for fully polarizable forcefields, in which case the time step had to be decreased from 1 fs to about 0.1 fs to accommodate the high vibrational frequencies of the core-shell units. The efficiency was improved by using the multiple time step, which allow to calculate the stronger interactions of close particles with higher frequency than weaker long distance interactions [57].

The initial configurations were usually constructed from equilibrated configurations of simpler systems. In the first step, we performed simulations of PEO melt starting from a disordered system of polymer chains, which was consequently compressed to the desired density, equilibrated at a higher temperature, and slowly cooled down to the target temperature. Then we set up our initial configuration for the simulations of PEO binary solutions by adding an appropriate number of ions (PEO/LiI mixtures) or water molecules (PEO aqueous solution) by removing randomly chosen polymer chains and inserting

ions or water molecules while avoiding overlaps. The number of water molecules and ions added was determined by the corresponding experiments. The configurations for ternary mixtures were created by adding water molecules to equilibrated configurations of the PEO/salt system. The precise composition of each system will be given in the following sections. Equilibrations were performed for approximately 1-2 ns for all simulations. Each system has 1-2 ns of production runs.

The starting point for the representation of physical interactions between atoms, ions, and molecules in our simulations was the set of forcefields developed by Smith et al for PEO, PEO/water, and PEO/LiI systems [6-10, 14, 16, 56]. They were used first in the simulations of binary systems, which tested our methods and evaluated the effect of polarization, and then provided a basis for the development of the forcefield for PEO/LiI/water mixture. The parameters for the potential functions for binary and ternary mixtures, the procedures employed for their optimization, and the results obtained will be given in the appropriate sections. In Section 4.2 and 4.3 we describe our simulations for pure PEO polymer and solid polymer electrolytes (PEO/LiI) respectively, followed by the discussion of our forcefield development on the PEO/water binary mixture in section 4.4. In the remaining Section 4.5, we present our results on the changes in both structure and dynamic properties of the polymer electrolytes when water is terms of present.

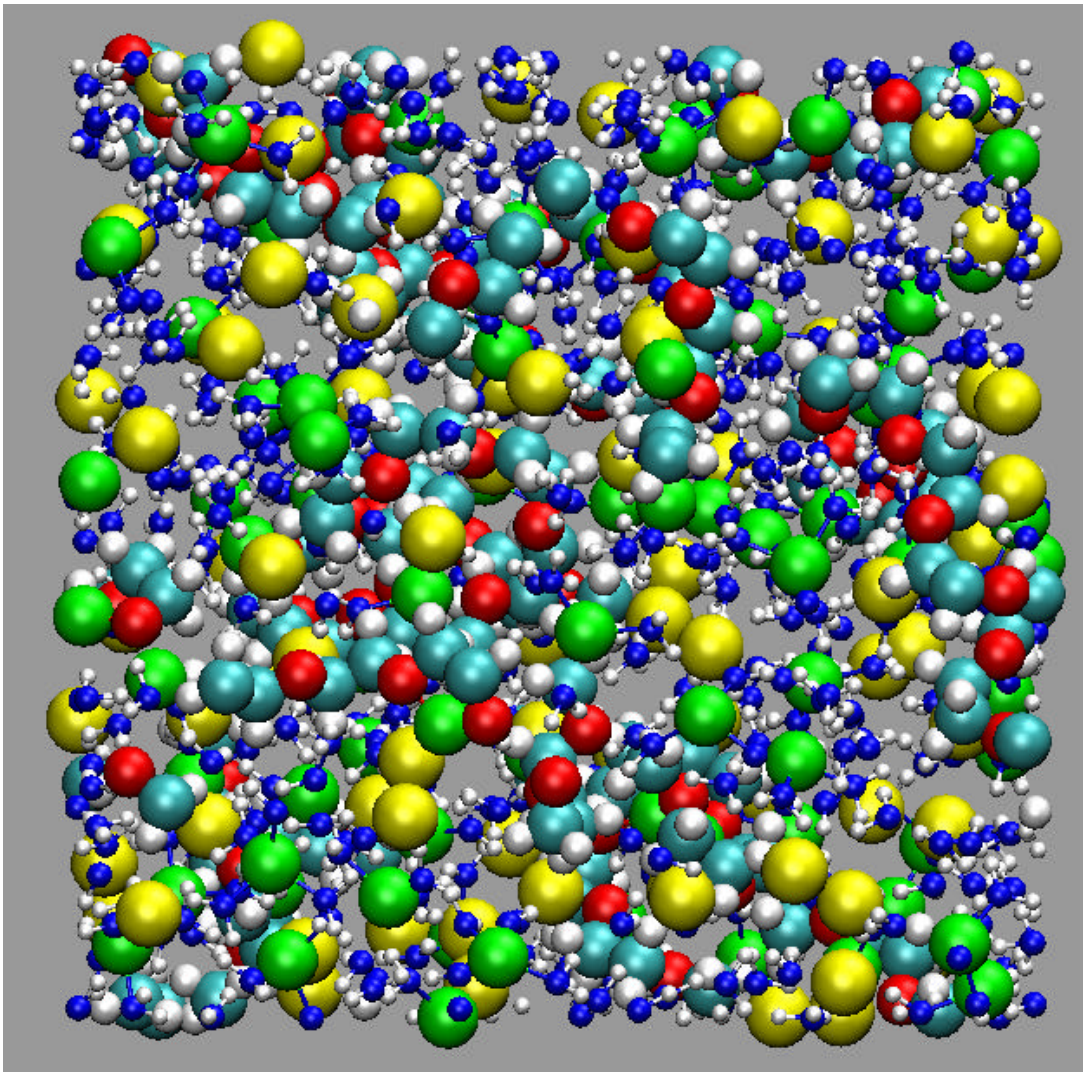

Figure 10: Ternary mixture PEO/LiI/water. Lithium (green), Iodine (yellow), carbon (cyan), ether oxygen (red), water oxygen (blue), and hydrogen (white). The size of water molecule atoms was reduced to enable the PEO, Li^+ AND I^- to be seen more easily.

4.2 PEO simulations

Since it is accepted that ion conductivity takes place predominately in the amorphous phase of the polymer host, we were only interested in the properties of the polymer melt, which means our simulation temperature was fixed above the melting point of PEO polymer, as in the work of Smith and coworkers [20].

The simulated PEO system was composed of 20 PEO chains with 54 ether units, i.e. - $(CH_2\text{-}O\text{-}CH_2)_{54}$- , resulting in a polymer molecular weight of 2800 Da. To be consistent with experiment [20], the NVT ensemble was used to keep the system density at 1.11 g/cm^3 and temperature at 363K. The interactions were represented by a non-polarizable model [14, 64], which is sufficient for pure polymer; adding explicit polarizability would only increase complexity without additional benefits.

Figure 11 presents the experimental and simulation results for the structure factor $S(Q)$ and total distribution function $G(r)$. The structure factor is calculated from [20]

$$\left(S(Q)-1\right)\bullet\ \langle b\rangle^2=\sum_i\sum_j c_i c_j b_i b_j\left(S_{ij}(Q)-1\right)\quad , \tag{44}$$

where the weighted average scattering length is defined as $\langle b\rangle=\sum_i c_i b_i$. The partial structure factors, $S_{ij}(Q)$, are the Fourier transforms of the partial distribution functions, $g_{ij}(r)$. See equation (9).

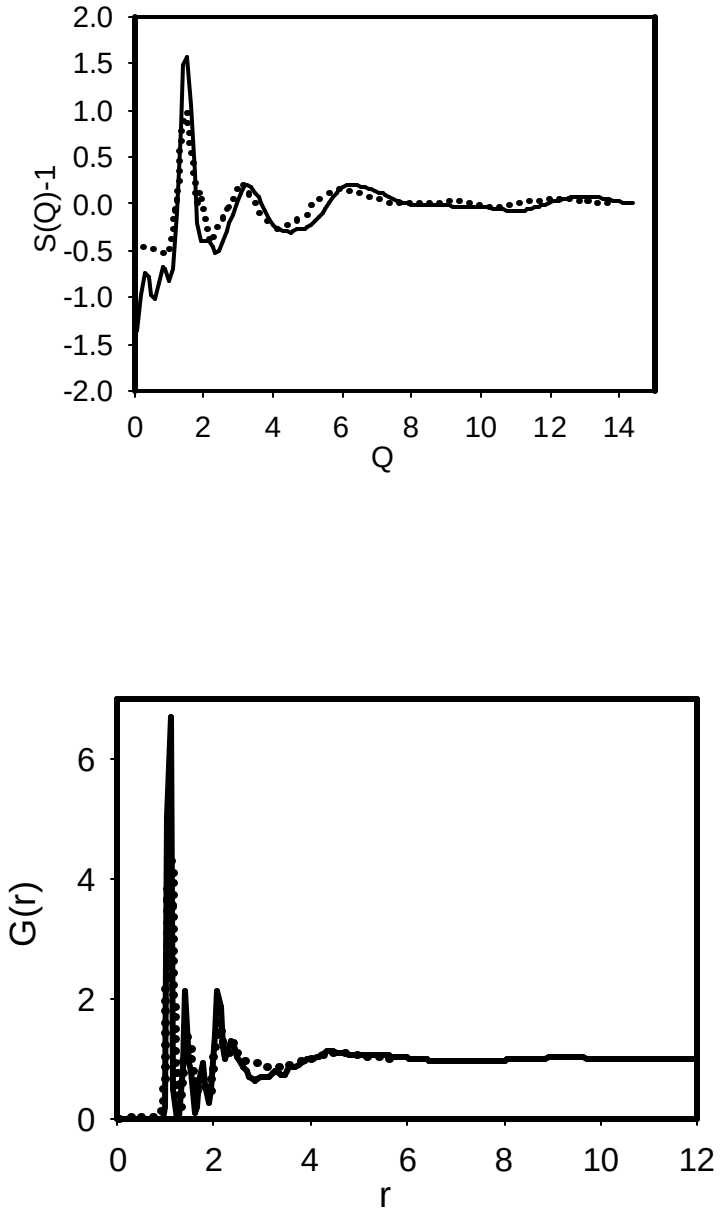

Figure 11: The total structure factor and correlation function of PEO melt calculated from simulations (solid line) and obtained from the NDIS experiment (dashed line) [20]

The total correlation function $G(r)$ is then defined as [20]

$$G(r)-1=\langle b\rangle^2\sum_i\sum_j c_i c_j b_i b_j\left(g_{ij}(r)-1\right) \tag{45}$$

It can be seen that the agreement is very good, with simulation results reproducing all the important features of the $S(Q)$ and $G(r)$ functions. These forcefields and systems were first considered by Smith and co-workers [20]. The agreement of our simulation results for the structural factor and total correlation function with their results, as shown in figure 11, confirms the correctness and accuracy of our simulation methodology. These simulations give us comprehensive information about the structure of polymer molecules in pure amorphous PEO and form the basis for the further investigation of PEO/salt and PEO/water binary systems.

4.3 PEO/salt simulations

To include the effect of polarizability in PEO/salt simulations, we performed molecular dynamics simulations of PEO/LiI systems using three forcefields that differed in the ways polarization effects are taken into account. This work is based on the forcefields developed by Smith's group [31]:

1) Forcefield_1: non-polarizable model

2) Forcefield_2: model including effective polarization between ions–polymer

and polymer-polymer. The potential parameters for these effective polarization are taken from the literature [73].

3) Forcefield_3: model including effective polarization in ion-ion, ion-polymer and polymer-polymer interactions, differing from the Forcefield_2 by the inclusion of averaged polarization effects between cations and anions. The potential parameters are taken from the literature [73].

To enable a comparison between simulations and available NDIS experiments and other simulations from the literature [31, 73-76], we simulated two mixtures with different compositions. Each of them was composed of 32 PEO polymer chains with 12 repeat ether units (MW=530 Da). Each mixture has 384 ether oxygens but differ in the ratios of ether oxygens (EO) to cations (Li^+), which were set at 5:1 (i.e., EO:Li=5:1) and at 15:1 (i.e., EO:Li=15:1) corresponding to 77 and 25 ion pairs, respectively. We simulated different systems using either the NVT or NPT ensembles, according to corresponding experiments [6]. For the system with high ion concentration (EO:Li=5:1), we used the NVT ensemble to keep system density at 0.87 g/cm^3 and temperature at 363K. For the system with low ion concentration, we used the NPT ensemble to fix the pressure at 1 atmosphere (yielding a final density of approximately 1.0 g/cm^3) and temperature at 363K.

Figure 12 shows the total distribution function, ΔG, which is defined as [31]

$$\Delta G(r) = 1 + \frac{A(g_{LiO} - 1) + B(g_{LiC} - 1) + C(g_{LiD} - 1) + D(g_{LiI} - 1) + E(g_{LiLi} - 1)}{\sum} \quad (46)$$

where, the coefficients are defined as:

$$A = 2C_{Li}C_O b_O \left(b_{Li-6} - b_{Li-Nat}\right) \quad (47)$$

$$B = 2c_{Li}c_c b_c \left(b_{Li}^6 - b_{Li}^{nat}\right)$$

$$C = 2c_{Li}c_D b_D \left(b_{Li}^6 - b_{Li}^{nat}\right)$$

$$D = 2c_{Li}c_I b_I \left(b_{Li}^6 - b_{Li}^{nat}\right)$$

$$E = c_{Li}^2 \left(\left(b_{Li}^6\right)^2 - \left(b_{Li}^{nat}\right)^2\right)$$

and

$$\sum = A + B + C + D + E \quad (48)$$

The structural results presented in Figure 12 are from the simulations of the system with the high ion concentration (EO: Li=5:1).

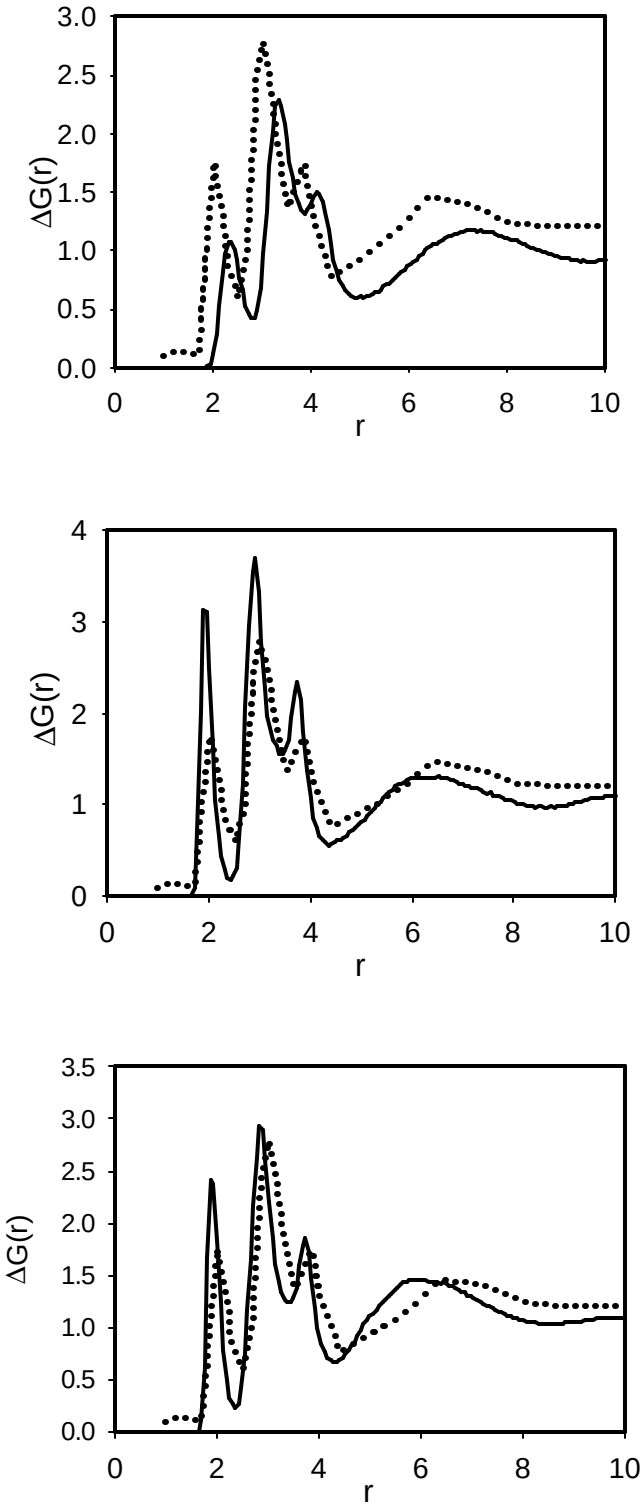

Figure 12: Total pair distribution function in PEO/LiI system with EO:Li=5:1 compared with result from NDIS experiments [31].

Figure 12 demonstrates how polarizability influences the structural properties of the simulated polymer electrolytes. The largest derivation between the simulation results and experiment data is obtained with the nonpolarizable forcefield (Forcefield_1), which underestimates the interaction between the ions and polymer and results in lower peak heights located at larger distances. The agreement with experiment is improved by including ion-polymer and polymer-polymer polarizability (Forcefield_2). In this simulation the peaks are shifted to smaller distances and are higher. The forcefield in which we include effective polarization effects between cations and anions (Forcefield_3) provides the best agreement with experiment [31].

To probe the dynamical properties, we calculated the ionic conductivity and self-diffusion coefficient of lithium ions using the fully polariziable forcefield (Forcefield_3). Table 4 compares simulation results with currently available experimental data and shows that they are within the same order of magnitude.

4.4 Polymer/water forcefield development

As mentioned earlier, there is evidence that polarization effects can be neglected in the simulations of binary PEO/water mixtures. However, we wanted to use both PEO and water in ternary mixtures composed of PEO polymer, water and

Table 8: Ionic conductivity and self-diffusion coefficient of Li^+. The simulations were performed using forcefield_3

System	Molecular dynamics simulation	Experiment
Ionic conductivity (EO:Li=5:1)	$3.4x10^{-5}$S/cm	$1.5x10^{-5}$S/cm [6]
D_{Li} (EO:Li=15:1)	$2x10^{-7}cm^2/s$.	$7x10^{-7}cm^2/s$* [76]

*Note: This value was obtained by interpolating experimental data to Mw=530 Da, the same Mw of PEO as used in our simulation [76, 77]

ions, where the polarization can be expected to be very important due to the presence of ions. Since no forcefield was available that would include explicit many-body polarization effects, we had to develop one by ourselves.

As was described in the previous chapter, there are two ways to approach this task: empirical and quantum chemical. We followed both of them and developed two forcefields: a simpler one, based on fitting empirical data, and a more complex one, based on *ab initio* calculations.

4.4.1 Empirical forcefield

The empirical forcefield was based on the PSPC model of water [62], which has a polarizable center located at the oxygen atom. To achieve a consistent and simple description of the system, we also included the polarizabilities of polymer hydrogens to the nearest heavy atom, i.e., carbon. Partial atomic

charges were maintained at values originally optimized for pure water and PEO. To derive the parameters of the remaining VDW interactions, we fitted the Buckingham potential of the polymer-polymer interactions with a Lennard-Jones potential and then used Lorentz-Berthelot combining rules to obtain cross interactions between polymer and water. However, we found that this forcefield overestimates the attractive interactions and, therefore, we proceeded by rescaling the repulsive part of the LJ potential so that the structure (pair distribution functions) of the binary polymer mixture corresponded to available experimental data. This procedure is analogous to the way the PSPC potential was derived from its nonpolarizable parent model (SPC) by rescaling the repulsive part of the non-Coulombic interactions [83]. The resulting LJ parameters for these interactions are given in the next section along with other parameters for the ternary mixture.This type of forcefield has two limitations. First, as discussed earlier in section 3.3, including the polymer-hydrogen polarizability into the polymer backbone atoms is an approximate approach and underestimates the quantum-chemistry-based molecular polarizabilities of DME or PEO [56]. Second, we used a simplified Lorentz-Berthelot combing rule to calculate the cross term interaction parameters between PEO and water. The results obtained with this forcefield are presented in Section 4.5.2

4.4.2 *Ab initio* forcefield

Given the uncertainties related to empirical forcefields, we proceeded one step further and derived the parameters of the VDW cross interactions from quantum chemical calculations, while maintaining polarizable centers on all atoms including water and polymer hydrogens. The basis for the PEO model was the fully polarizable *ab initio* forcefield developed by Smith et al [56], and water was represented by the RPOL model [63], which has a consistent form with polarizable hydrogens. The partial charges and atomic polarizabilities were retained at values optimized for pure water and PEO. VDW cross interactions had to be optimized using data from *ab initio* calculations of a water-polymer dimer.

Since quantum chemical studies of large systems are computationally demanding and we are interested in short range VDW interactions, we used a short DME molecule, which has the same local conformational properties as long PEO chains. The procedure we employed in this work follows closely the one Borodin et al. used for the development of a non-polarizable water-DME/PEO forcefield [64].

To obtain data for fitting and optimization, we performed *ab initio* energy calculations for a DME-water complex at selected configurations as a function of the distance between the two molecules. The calculations were

performed using the public domain software NWCHEM. We focused on the interaction of water with the *trans-gauche-trans* (tgt) conformer of DME, which is the most probable conformer of DME and PEO in aqueous solution [64]. The selected configurations were arranged into two series, one forming a hydrophilic and one forming a hydrophobic path, as shown in Figure 13a and 13b. The hydrophilic path represents configurations that can be created when a water molecule is forming hydrogen bonds to two ether oxygens. While unlikely to form naturally between two molecules in the gas phase, the configurations of the hydrophobic path are included to obtain a wider range of water-DME interactions, providing a better description of all possible situations in the solution. The geometry of the dimer path was optimized at the B3LYP/aug-cc-pvDz level at the most favorable water-DME configuration for each path. Then the geometry of both molecules was fixed and the only parameter that changed was their mutual distance. The energy calculations used the same basis set (aug-cc-pvDz) and were performed at two levels. The HF level, which does not account for dispersion interactions, was used to optimize the repulsive part of the VDW potential, and the MP2 level was used to estimate the dispersion interactions by extrapolating interaction energies from HF and MP2 to the infinite order of MP perturbation method.

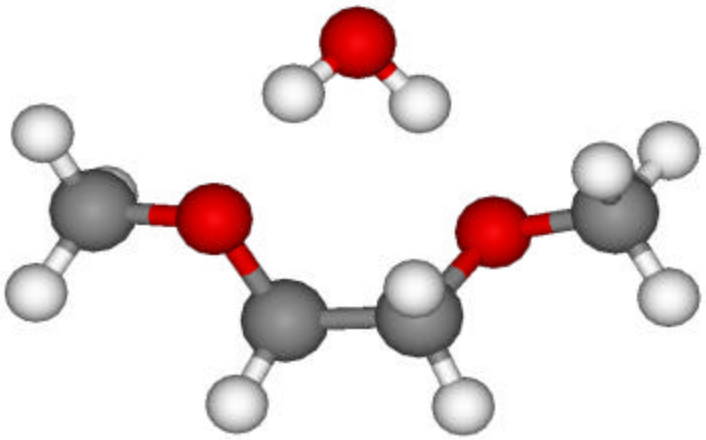

a: Hydrophilic binding

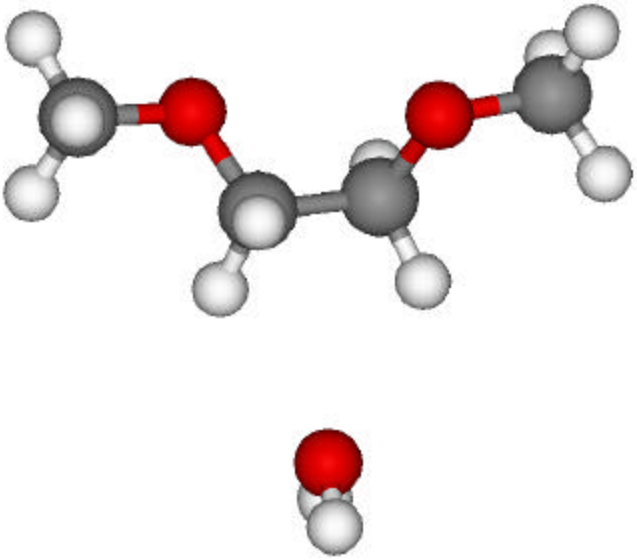

b: Hydrophobic binding

Figure 13: Optimized DME- water complex

We were only interested in the parameterization of the intermolecular non-bonded interactions between water and PEO, which can be split into atom core repulsions, attractive dispersions, and electrostatic interactions, where the non-Coulombic part can be cast in the form of the Buckingham potential (see section 3.3). First, we used the HF level calculations and fit the results with the exponential repulsive part of the Buckingham potential. Because the fit was not very good, we followed the procedure outlined in Borodin *et al.* and added a special potential function to describe hydrogen bonding interactions between water hydrogens and ether oxygens, of the form [64]:

$$U^{HB}\left(r_{ij}\right) = -A_{ij}^{HB}\exp\left(-B^{HB}r_{ij}\right) \tag{49}$$

Having optimized all repulsions and attractive hydrogen bonds, we determined the dispersion interactions and fit them with the usual form of the inverse sixth power function. Figure 14 shows the *ab intio* energies of the DME-water complex as the function of a distance between these molecules and compares them with the results from the forcefield using our optimized parameters. All parameters are listed in Tables 9 and 10.

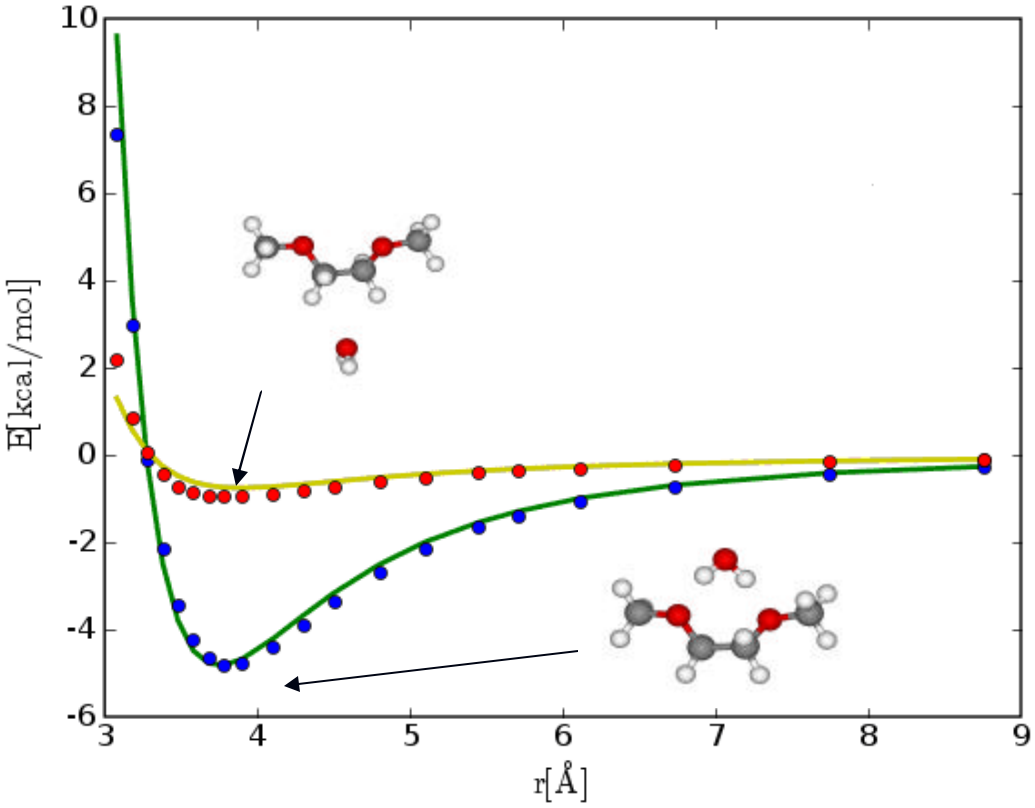

Figure 14: Fitting of non-Coulumbic interactions between water and DME. The circles are the results taken from *ab initio* calculation (blue circle: hydrophilic, red circles: hydrophobic). The solid lines are results take from simulations using fitted parameters(green line: hydrophilic, yellow line: hydrophobic)

Table 9: Parameters for DME-water nonbonded interactions:

Atom pair	A(kcal mol -1 Å^{12})	C(kcal mol -1 Å^{6})
Ow-O	896877.2	1033.49
Ow-C	308055.62	127.038
Ow-H	78754.04	137.374

Table 10: Parameters for DME-water hydrogen-bond interactions:

Atom pair	A^{HB} (kcal/mol)	B^{HB} (kcal/mol)
Hw-O	-19.0581	1.5424

To test the quality of our new parameters and forcefield, we performed a series of molecular dynamics simulations of the aqueous solution of DME at different concentrations. Using the NPT ensemble the system was kept at 318K and 1 atmosphere. We compared the excess volume of the mixture obtained from simulations and experiments. The results shown in Figure 15 demonstrate that our *ab initio* forcefield is capable of reproducing the density variations very well.

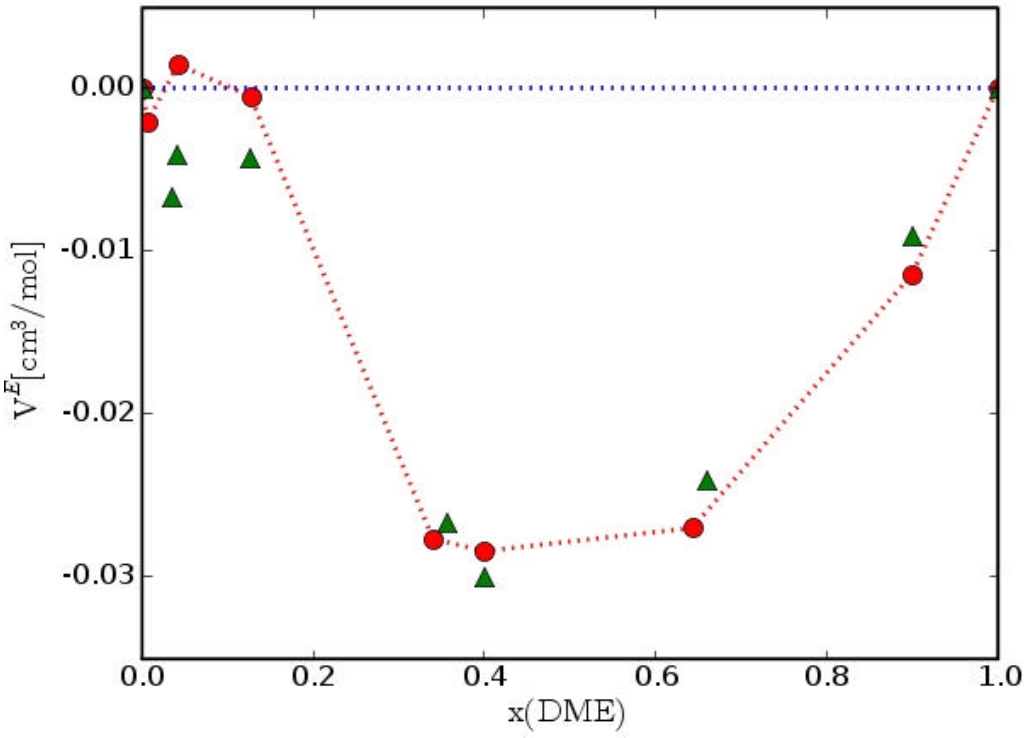

Figure 15: Comparison of excess volume of water/DME mixtures obtained from molecular dynamics simulations (dashed line) using *ab initio* forcefield and experiment (triangle) at 318 K as a function of solution composition

4.5 PEO/salt/water simulations

The core of our work is the study of the ternary PEO/LiI/water mixture and the influence of water content on ion conductivity. To choose the appropriate model for the simulations, we first test the effect of polarization on the structure in the way similar to which we used for the binary PEO/LiI mixture. Then we proceeded to simulations with two fully polarizable forcefields incorporating PEO-water interactions introduced in the previous chapter.

In the first step, we tested several forcefields by comparing the predicted structure around lithium ions to available NDIS experiments [21]. To insure consistent conditions, we used the NVT ensemble to keep the system density ($1.68 g/cm^3$) and temperature (298K) at the experimental values. To compare with corresponding NDIS experiments, the composition of our system was set to 6 deuterated polymer chains with 12 repeat ether units and 77 LiI ion pairs in aqueous solution (499 D_2O molecules), giving the ratio of cations to ether oxygens to water oxygens approximately 1:1:6. In the next step, we used the best forcefield to study the details of molecular structure and mobility of lithium in mixtures with more realistic compositions. These simulations were carried out in the NPT ensemble at standard ambient conditions.

4.5.1 Pair additive forcefields

As in the previous study of the PEO/LiI system [31], we used three different forcefields to test the degree, to which polarization influences the environment of ions in PEO aqueous solution:

1) Forcefield_1: non-polarizable model

2)Forcefield_2: model including effective polarization between ion/polymer and polymer/polymer pairs. The potential parameters are taken from literature [73]. Water was represented by the non-polarizable SPC/E model. There is no effective polarization included for water-ion and water-polymer.

3)Forcefield_3: model including effective polarization in ion-ion, ion-polymer and polymer-polymer interactions and so differ from Forcefield_2 by including averaged polarization effects between cations and anions. The non-polarizable SPC/E model was used to represent water. There is no effective polarization included for water-ion and water-polymer interactions.

In the same way that we analyzed polarization effects in the PEO/LiI system [31], we performed three sets of simulations using the above mentioned potential models and the total distribution functions for Li ions are shown in Figure 16. Simulations using the non-polarizable forcefield (Forcefield_1) predicted two peaks at 1.95-2.0 ? and 2.61-2.65 ?, identified as corresponding to Li-water oxygen and Li-water hydrogen and in a good agreement with

experiments [21, 78-79]. However, this forcefield may underestimate interactions between ions and polymer chains because it does not include the polarization effects, seen in the simulations of binary PEO/LiI mixture using the non-polarizable forcefield as the presence of more cations in water than observed experimentally or in lower lithium-ether oxygen distribution peak from simulations. Using a model that incorporates effective polarization between ions and polymer (Forcefield_2) seems to correct the situation to a certain degree and increases the ion polymer bonding as is indicated by slightly lower first two peaks corresponding to ion-water binding. However, when the effective polarization is incorporated into all pair interactions, including water and ions (Forcefield_3), the predicted distribution functions are not satisfactory. The first two peaks of $G_{Li}(r)$, representing the first shell of hydration around lithium, have much lower peak heights than the NDIS experimental results, which can be explained by the underestimation of interactions between water and ions. The disagreement is probably due to our approximate treatment of cross interactions based on simple combining rules, which may not be adequate. The results strongly suggest that a simple combination of effective polarizations is not a reliable approach for the study of complex mixtures and suggests the need for general many-body polarizable forcefields.

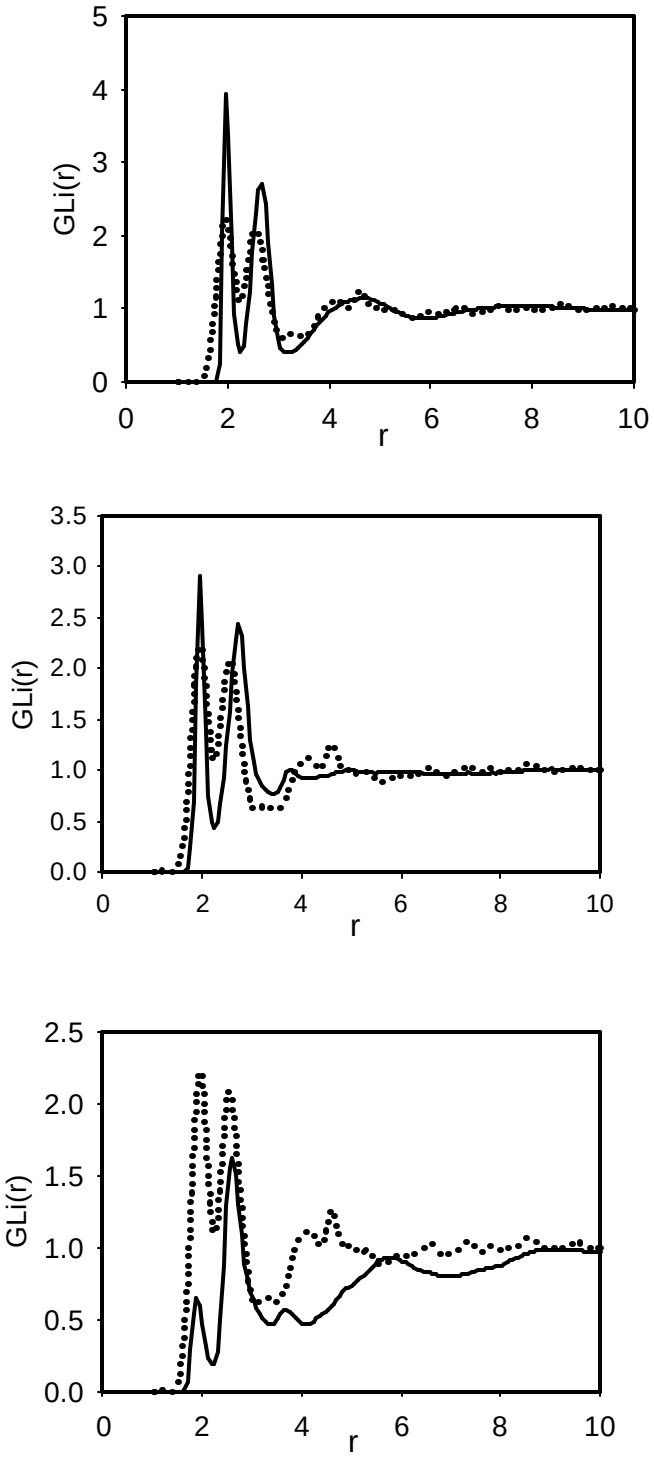

Figure 16: Total pair correlation function $G_{Li}(r)$ in PEO/LiI/water system from simulations compared with neutron scattering experiment data [21]. The PEO has molecular weight 580 Da, and the PEO:water:LiI ratio is 1:1:6.

4.5.2 Empirical polarizable forcefield

4.5.2.1 System definition

In Section 4.5.1, we used SPC/E water model and an effective polarizable forcefield to prove the importance of polarization for the simulation of the ternary mixtures of PEO, ions and water. In this section we will describe our methodology for the development of a many-body polarizable forcefield. In the first version of our many-body polarizable forcefield the core-shell units of the dynamic shell model were placed on the polymer oxygens and carbons (the polarizabilities of hydrogen atoms are included in the heavier atoms). We used a quantum chemistry-based forcefield for PEO developed by Smith et al. [56] and for water we used the polarizable simple point charge model (PSPC) [62] consisting of three atomic interaction sites, with a Lennard-Jones (LJ) center and a polarizable center placed on the oxygen site. All ions were represented by point charges with a LJ center, with parameters taken from Dang et al [80-82]. Polarizability was only assigned to iodide ions since lithium cations are almost non-polarizable (a_{Li} =0.024Å^3). Atomic charges and polarizabilties, taken from simulations studies of pure PEO polymer and ions [56, 63, 81-83] and used in the fully polarizable forcefield, are listed in Table 6. The equations of motion were integrated with 0.4fs time step, using multiple time scale methodology to

calculate stronger interactions as described earlier.

Table 11: Polarizabilities and charges of atoms [56, 63, 81-83]

Atom type	Polarizability α_i Å^3	Charge q_i e	Core charge	Shell charge	Spring constant kcal/mol*Å^2
O(ether)	0.748	-0.2792	1.0000	-1.2792	726.4
C(-CH_3)	1.874	-0.1187	2.0000	-2.1187	795.4
C(-CH_2)	1.874	-0.0326	2.0000	-2.1187	732.9
Li	0.024	1	NA	NA	NA
I	10.042	-1	1	-2	127.7
O(water)	1.44	-0.6690	-3.75141	3.08241	2193
H(water)	NA	0.33450	NA	NA	NA

Table 12: Lennard-Jones potential parameters [81-83]

Atom pairs	ε_{ij} [kcal/mol]	σ_{ij} [Å]
Li-Li	0.165	1.506
I-I	0.1	5.167
O(water)-O(water)	0.1295	3.263

Table 13: Repulsion (A) and dispersion (B and C) parameters for the PEO

Atom pairs	A [kcal/mol]	B [1/?]	C [kcal/? ^6mol^1]
C-C	14976.0	3.09	595.94
C-O	33702.4	3.577	470.18
C-H	4320.0	3.415	128.56
O-O	75844.8	4.063	370.96
O-H	14176.0	3.9015	97.16
H-H	2649.6	3.74	25.44

4.5.2.2 Structural properties

Figure 17 shows the comparison of the total distribution function around lithium ions, $G_{Li}(r)$, between our molecular dynamics simulations and the NDIS experiment [21]. Both of them exhibit the first two peaks located at 1.95-1.98 and 2.62-2.66 Å, identified as the distributions of oxygen and hydrogen atoms of the nearest-neighbor water molecules, respectively. Previously reported simulations of aqueous inorganic solutions, such as LiCl in water, found very similar peaks located at 1.96-2.12 for Li-O and 2.52-2.61 Å for Li-D [78-79]. To calculate the number of water molecules in the first coordination shell of Li^+, we followed [21] and integrated the total distribution function from 1.5 to 3.0 Å, thus covering the first two peaks. We found 3.2 water molecules presenting in the coordination shell in both simulation and experiment. Studies of aqueous

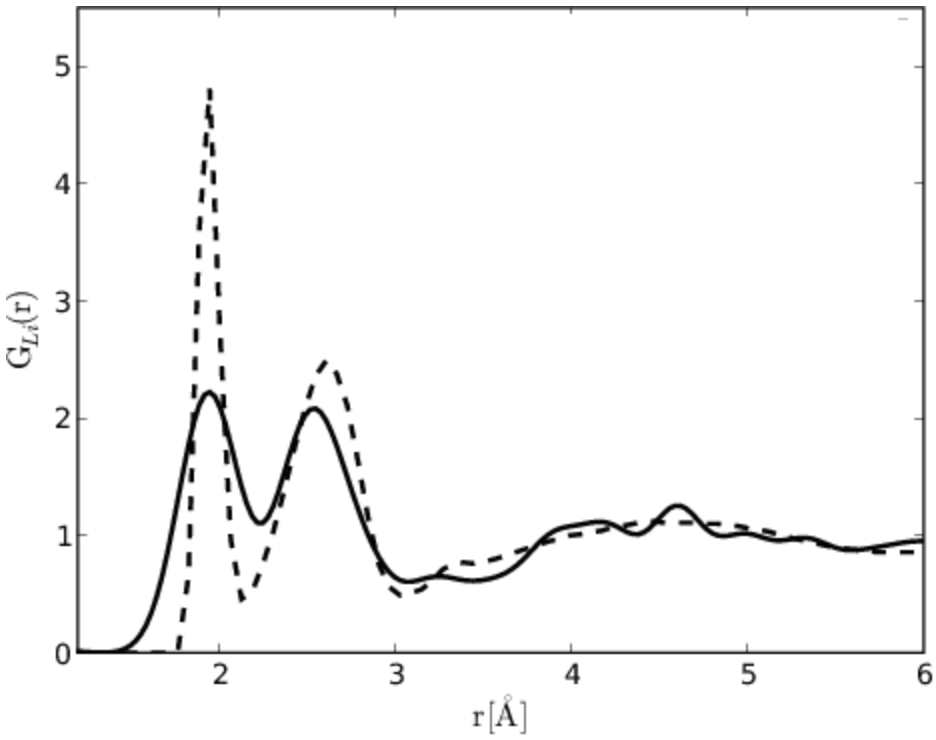

Figure 17: Total distribution function for lithium ions, G_{Li}. Comparison of MD simulations (dashed line) with experimental results (solid line) [21].

inorganic solutions with similar ratios of water molecules to cations yield similar solution structure around the Li ion, suggesting that the PEO in PEO/LiI/water solutions does not have a large influence on the hydration of Li ions. Both molecular dynamics simulation and experiment thus suggest that in the ternary mixtures more lithium ions are found to decouple from the polymer chain and are in close proximity to the water oxygen [21]. This situation is illustrated in a simulation snapshot in Figure 20, where the majority of ions can be seen to be detached from polymer chains.

To obtain more detailed insight into the ion environment, we also directly calculated the Li^+ - water oxygen pair distribution function and its integral according to [21]

$$N(R) = 4\pi r_a \int_0^R r^2 g_{Lia}(r)\, dr \qquad , \tag{50}$$

where r_a is the number density of water oxygens. Both results are shown in Figure 18. The analysis shows that there are 3.6 water molecules within the first hydration shell (R<2.5?) and the remaining valence is saturated by the average of 0.3 ether oxygens and 0.1 I^- anion. Li^+ ions are thus in a very similar environment to that in pure water. As our complementary simulations have shown, Li^+ ions in binary PEO/LiI melt are surrounded by 3.5 ether oxygens and the remaining valence is saturated by 0.5 I counter ions. Addition of water breaks most of these bonds, saturating the cation valence. Free ether oxygens

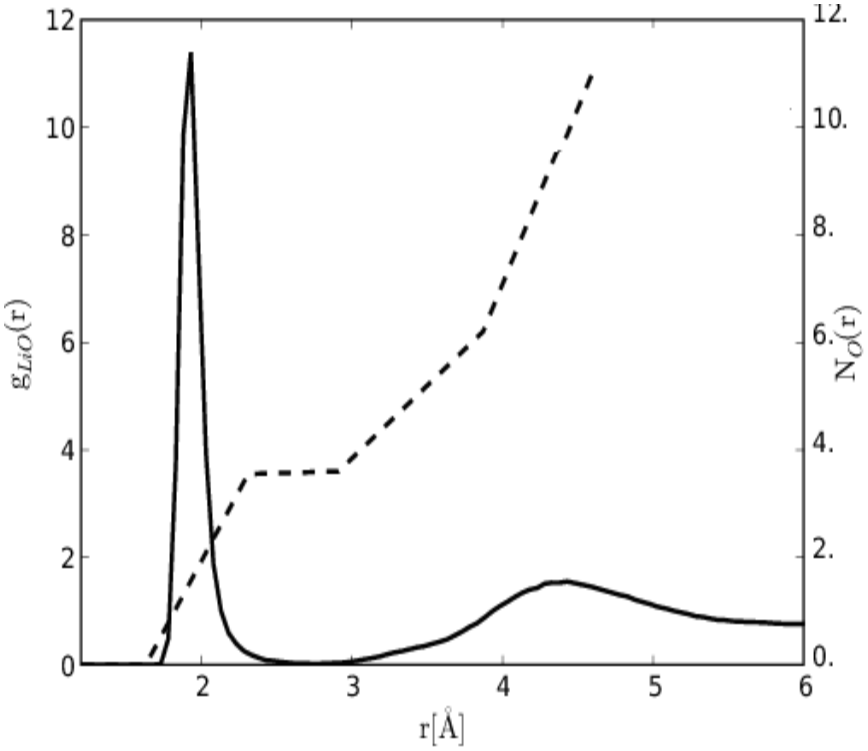

Figure 18: Li^+ ion – water oxygen pair distribution function, $g_{LiO}(r)$, (solid) and its integral, $N_O(r)$, (dashed) from molecular dynamics simulations.

form on average 1.6 hydrogen bonds with water hydrogens and provide them with an almost tetrahedral environment. These interactions are documented in Figure 19 showing ether oxygen-water hydrogen distribution function and its integral computed according to equation (45). The hydration of PEO/LiI mixture also results in the straightening of polymer chains, which are no longer curled around Li^+ ions. These changes, along with the separation of cation-anion pairs, are most likely behind the observed substantial increase in ionic conductivity. The coordination numbers of Li^+ ions in binary and ternary mixtures are summarized in table 9 along with diffusivities of Li^+ ions in these environments. We notice that in the studied ternary mixture most cations are surrounded by water, but the ratio of different ligands in the first coordination shell roughly corresponds to the ratio of concentrations of these atoms. The simulations thus suggest that while water successfully competes with other ligands, modifies the lithium environment, and changes the structure of the polymer, at low water concentrations (which are more interesting from the practical point of view) Li^+ will be still strongly influenced by PEO ether oxygens. Further analysis shows that most lithium ions in our ternary mixture are coordinated by four water oxygens but some of them are coordinated by three or four ether oxygens. Such a situation is demonstrated in the simulation snapshot shown in Figure 20.

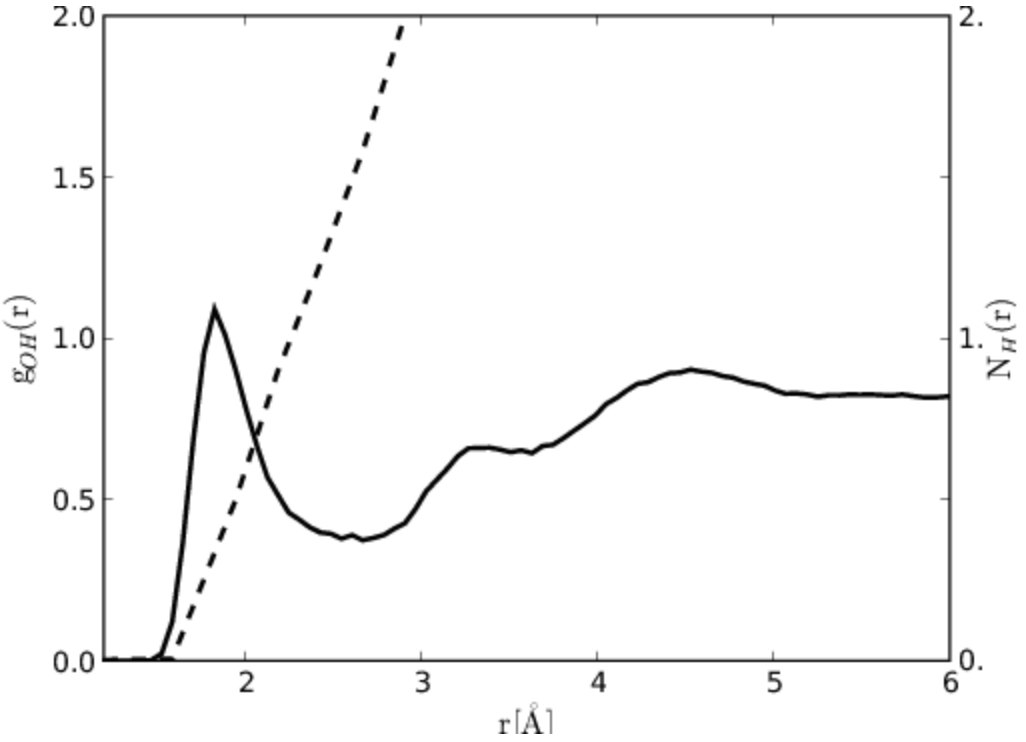

Figure 19: Ether oxygen-water hydrogen pair distribution function , $g_{OH}(r)$, (solid) and its integral, $N_H(r)$, (dashed) from molecular dynamics simulations.

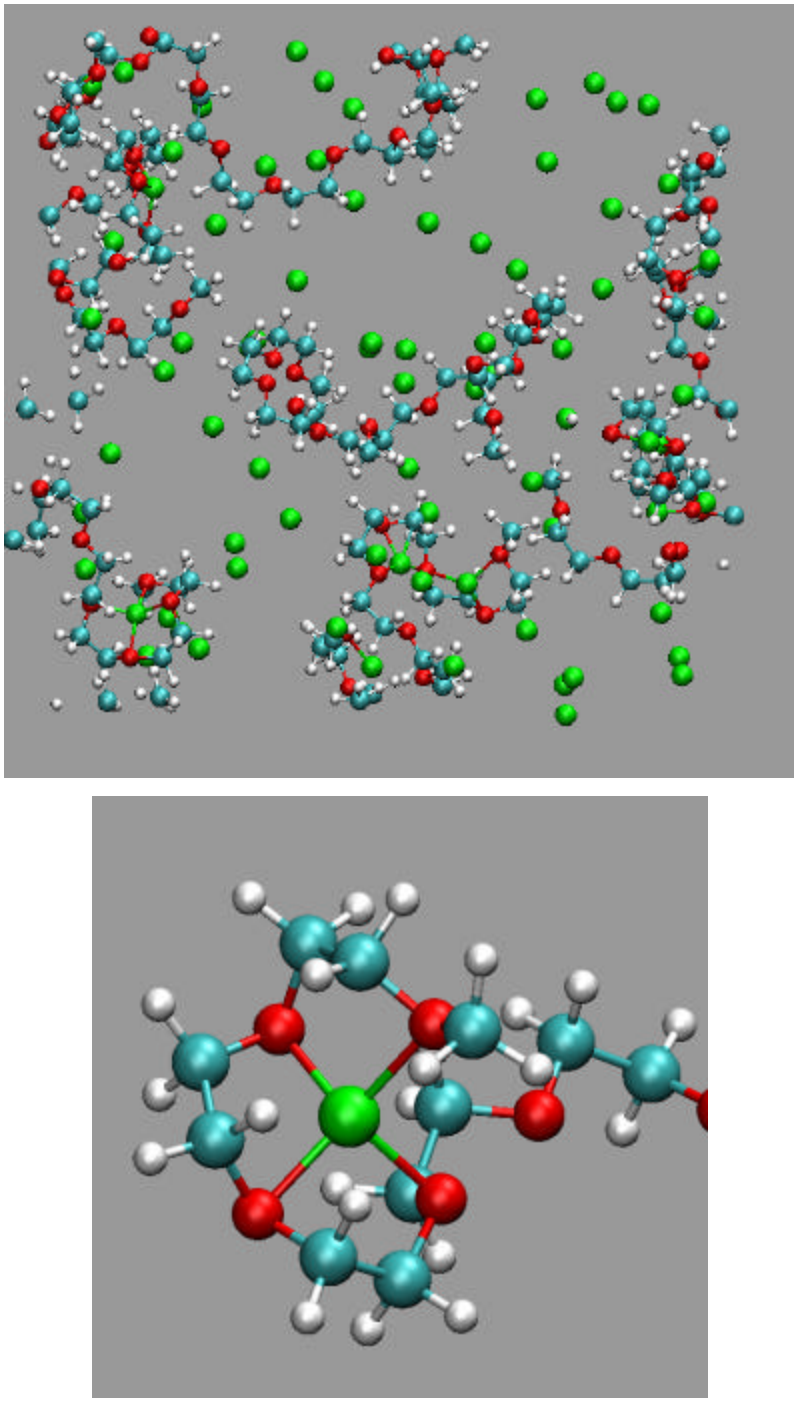

Figure 20: Simulation snapshots of PEO/LiI/water mixture showing only Li^+ (green) and PEO (O: red, C: cyan, H: white). Top: View of the whole simulation box, demonstrating Li^+ ions are present mostly in the aqueous environment. Bottom: A close-up showing a chelate complex formed by Li^+ and PEO.

Mixed coordination shells are rare. We note that the relative success of PEO in the complexation of lithium ions can thus be ascribed to the chelate effect, which stabilizes the complexes despite weaker interactions with individual ether oxygens. As for the diffusivity of Li ions, we notice that while it is approximately 50 times larger in the ternary mixture than in the pure polymer, it is only about 1/4 of the value in pure water. Since most ions are surrounded by water, the results suggest that polymer molecules still inhibit the dynamics of ions by constraining the whole aqueous environment and constraining it through hydrogen bonds between ether oxygens and water hydrogens [83].

Table 14: Lithium coordination numbers and diffusivities in different mixtures

Ligands	Water/LiI (6.4:1)	PEO/LiI (5:1)	PEO/Water/LiI (0.9:6.5:1)
Water oxygen	4.0	NA	3.6
Ether oxygen	NA	3.5	0.3
Iodide	0.0	0.5	0.1
Diffusion coefficient [10^{-4}cm2/s]	0.0505	0.0002	0.012

Note: Numbers in parentheses give the ratios of appropriate ligands in the mixture.

4.5.3 *Ab initio* polarizable forcefield

4.5.3.1 System definition

We have seen that the empirical forcefield was capable of reproducing experimental results and provided useful insights into the structure of PEO/LiI/water ternary mixtures. In this section we precede one step further and improve the many-body polarizable forcefield by adding polarizable sites to all hydrogens and use *ab initio* optimized water-PEO potential functions. As a water model, we used the revised polarizable water model (RPOL) [63] instead of the PSPC water model used for the empirical forcefield. The RPOL model, introduced in Section 3.5.3, consists of three atomic interaction sites, each being polarizable and bearing a partial charge. The oxygen center also carries a Lennard-Jones (LJ) center. All ions were represented by point charges with a LJ center, with parameters taken from Dang et al. [81-82] with polarizability only assigned to iodide anions. Parameters for PEO/ions and RPOL/ions cross interactions were taken from the literature [81-82]. The optimization of forcefield parameters for PEO/RPOL cross interactions was described in Section 4.4.2. The *ab initio* optimized parameters for the PEO/RPOL cross interactions are listed in table 9. We studied several ternary mixtures with different ratios between the three components. One mixture had composition corresponding to that used in neutron scattering experiments with ratios between lithium ions,

ether oxygens, and water oxygens of 1:1:6.4 [21]. The PEO polymer studied has a molecular weight of 580 Da. Another series of simulations with lower salt and water concentrations, which were more realistic with respect to potential applications as polymer electrolytes, was studied at ratio between lithium ions and ether oxygens $Li:O_E$ = 1:5, and $Li:O_W$ ratio ranged from 1:0 to 1:6. All simulations were performed at ambient conditions. The NPT ensemble was applied to keep the system temperature at 298.15 K and pressure at 1 atmosphere.

4.5.3.2 Structure

Since the structural properties of the mixture were discussed in the previous subsection and the results obtained with the *ab initio* forcefield do not differ significantly, we focus mainly on the dynamic properties, such as lithium diffusion or conductivity. However, before proceeding to the dynamic studies, it must be verified that the present forcefield can properly describe the structure of the ternary mixture. For this purpose, we ran simulations with the composition of the ternary mixture corresponding to that used in neutron experiments, which was also used to test the empirical forcefield. The total distribution function for lithium from simulations and experiment is shown in Figure 21. It is seen that the positions of the first two peaks are slightly shifted

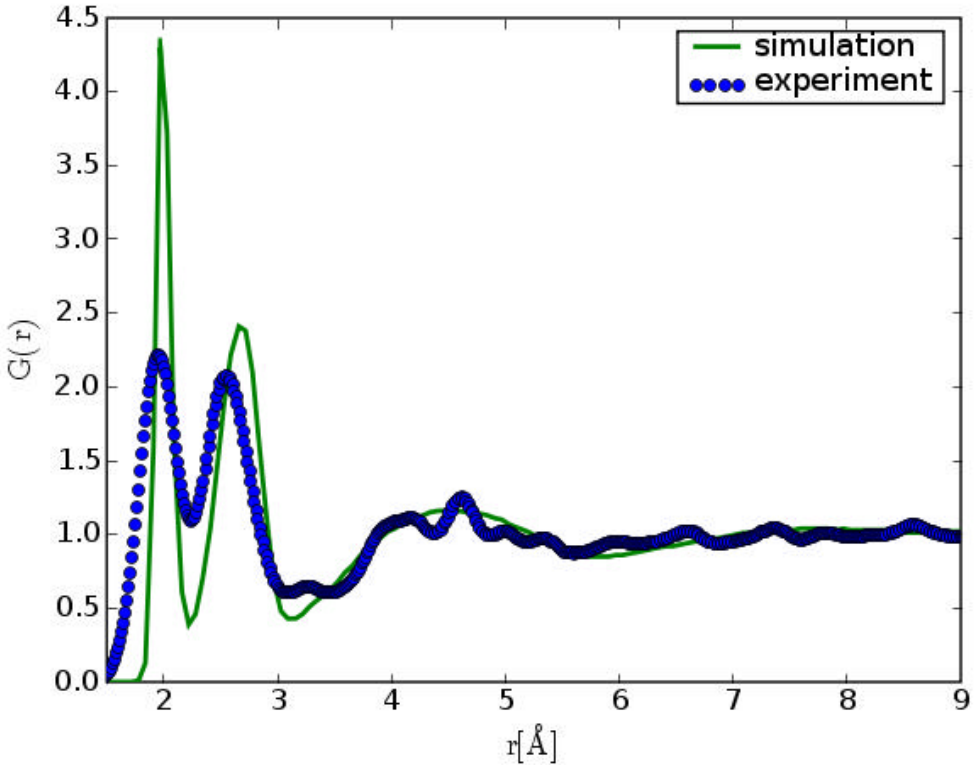

Figure 21: The total distribution function of lithium from simulations and NDIS experiment [21]

to larger distances and the peaks are taller and narrower. This effect indicates that the repulsive part of lithium-water potential is steeper than would correspond to the real system, but the overall trend of ions preferring aqueous environment is still correct.

As in the case of the empirical forcefield, we analyzed coordnation of lithium to surrounding oxygen atoms and iodide anions. The coordination numbers are summarized in Table 15. In the case of the mixture with the highest content of water ($Li:O_E:O_W$ = 1:1:6.4), almost all lithium ions are surrounded by four water molecules and only a small fraction is bonded to ether oxygens on PEO chains. Further analysis confirmed that the bonds to ether oxygens are stabilized by the chelate effect. In mixtures with high polymer concentrations, where the ratio of $Li:O_E$ is 1:5, there are enough ether oxygens to saturate all Li^+ ions with four bonds. The analysis of lithium coordination in Table 15 shows that if water concentration does not considerably exceed ether oxygen concentration, lithium ions will form complexes almost exclusively with polymer. Even at the ratio of ether to water oxygens of 5:6, lithium ions are preferentially bonded to PEO chains. The distribution of lithium ions between polymer and water environments for this concentration is illustrated in Figure 21. It is seen that the bonding environment of Li^+ is essentially reversed compared to the mixture with higher water concentration shown in Figure 19. A linear extrapolation of the number of water oxygens coordinated to Li^+ to higher water

concentrations for mixtures with $Li:O_E$ = 1:5 yields much lower values than are actually observed in the system with $Li:O_E:O_W$ = 1:1:6.4. It is not likely the result of different $Li:O_E$ ratios in these systems but rather the changes in the polymer configurations as more water is added to the system. At higher water concentrations, PEO chains become untangled and straighter as is seen in Figure 22 and SAXS (small angle X-ray scattering) experiments [84], reducing their ability to surround lithium ions and form chelate type of complexes. These changes are also reflected in the bonding of water hydrogens which is reported in Table 16. While at low water concentrations they are mostly engaged in bonding to iodide ions and water molecules, because ether oxygens are used-up by lithium, at high water concentrations they almost completely saturate all ether oxygens with two hydrogen bonds.

Since the chelation of Li^+ ions by PEO is driven entropically whereas solvation by water is driven enthalpically, the complexation can be, in principle, probed by calorimetric experiments. To our knowledge, no such experiments have been reported. The observed changes in the lithium coordination are naturally reflected in the mechanism of diffusion and ionic conductivity.

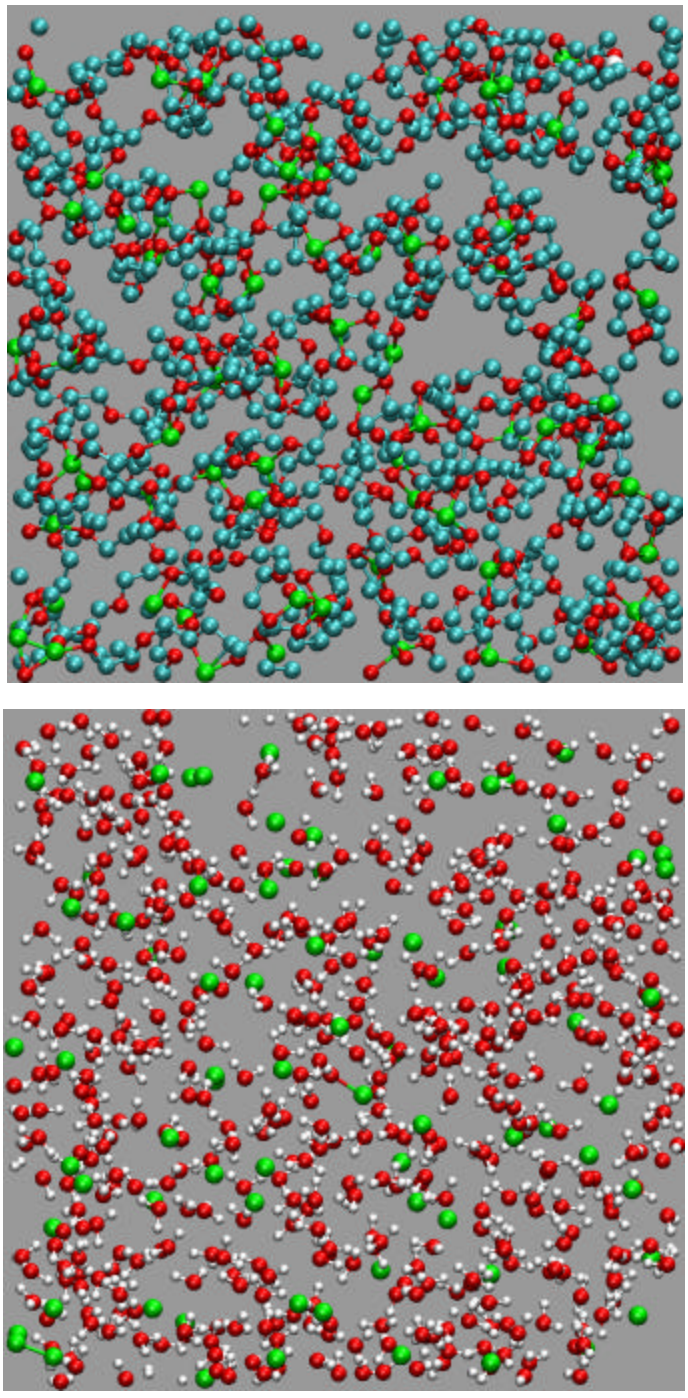

Figure 22: Simulation snapshots of PEO/LiI/water mixture ($Li:O_E:O_W$ = 1:5:6) showing Li^+ distribution in PEO (top) and water (bottom). Li: green, O: red, C: cyan, H: white.

Table 15: Average numbers, N, of ether oxygens (O_E), water oxygens (O_W), and iodide anions (I) coordinated to lithium cations (Li) in studied ternary PEO/LiI/RPOL mixtures.

$Li:O_E:O_W$	N_{OE} (ether oxygen)	N_{OW} (water oxygen)	N_I (iodide)
1:5:1 [a]	3.7	0.08	0.273
1:5:1.5 [a]	3.6	0.17	0.196
1:5:2 [a]	3.5	0.2	0.226
1:5:2.5 [a]	3.6	0.23	0.217
1:5:3 [a]	3.58	0.221	0.222
1:5:6 [a]	3.5	0.3	0.17
1:1:6.4 [b]	0.07	3.97	0.1

[a]) 77 LiI 32 PEO chains with 12 repeated units (32*12=72 ether oxygens),

[b]) 77 LiI 6 PEO chains with 12 repeated units (6*12=72 ether oxygens)

Table 16: Number of water hydrogens bonded to water oxygens (O_W), ether oxygens (O_E), and iodide anions (I) in studied ternary PEO/LiI/RPOL mixtures.

$Li:O_E:O_W$	H_W / O_W	H_W / O_E	H_W / I
1:5:1	0.584	0.11	0.72
1:5:1.5	0.641	0.14	1.21
1:5:2	0.707	0.158	1.61
1:5:2.5	0.823	0.25	1.63
1:5:3	0.834	0.33	1.97
1:5:6	1.09	0.22	3.7
1:1:6.4	0.84	1.9	6.0

4.5.3.3 Dynamics

Figures 23 and 24 and Table 16 show the calculated diffusion coefficient and conductivity of Li^+ ions as a function of relative water concentration (ratio of water oxygens to lithium ions) for the systems with $Li:O_E$ ratio of 1:5. In the range from 0 to 3 water molecules per lithium the diffusivity and ion conductivity of lithium ions increases approximately ten times. We notice that Li^+ conductivity in binary PEO/LiI obtained with the *ab initio* forcefield is approximately four times smaller than with the empirical forcefield, and in the same order of magnitude as experimental values of 10^{-5} S/cm [3]. On the other hand, we have seen that the average environment, as expressed by coordination numbers in Table 15, does not change very much; Li^+ ions are surrounded by approximately 3.6 ether oxygens, which is comparable to the bonding situation in a binary PEO/LiI mixture. There are at least two possible mechanisms which could explain such an increase in mobility: (i) Water molecules act directly on ions and facilitate their jumps from one PEO complex to another. Since the average number of water oxygens coordinated to lithium ions is very low, such complexes would be only transient. (ii) Another possibility for water to increase ionic mobility is through changing the conformation of the polymer chains. We have seen that at very high water concentrations (Figure 20) PEO molecules unfold and straighten due to the formation of hydrogen bonds to water. Even at

lower concentrations hydrogen bonding of PEO chains can result in the formation of complexes with decreased stability and lower activation energy for ionic diffusion.

The diffusion mechanism of Li^+ ions in a ternary mixture with high water content (1:1:6.4), where ions are surrounded almost exclusively by water, is very similar to the diffusion in pure water. The tenfold decrease in conductivity compared to pure water can be explained by the occasional formation of chelate complexes with PEO (Figure 24) and, more importantly, by the constriction of whole water domains through hydrogen bonding to the skeleton of the polymer chains. To achieve a substantial improvement in the ionic conductivity, water concentration must reach values high enough to saturate most of the PEO oxygens with hydrogen bonds. The analysis in Table 17 shows that ether oxygens can form more than one hydrogen bond and prefer tetrahedral coordination. Theoretically, each ether oxygen can immobilize up to two water molecules. Once all ether oxygens are saturated, water begins to form domains, which provide sufficient flexibility for easy ion diffusion. At the same time, however, mechanical stability, as one of the key advantages of SPE's, may be compromised. A possible solution to this problem may involve optimization of the PEO chain lengths.

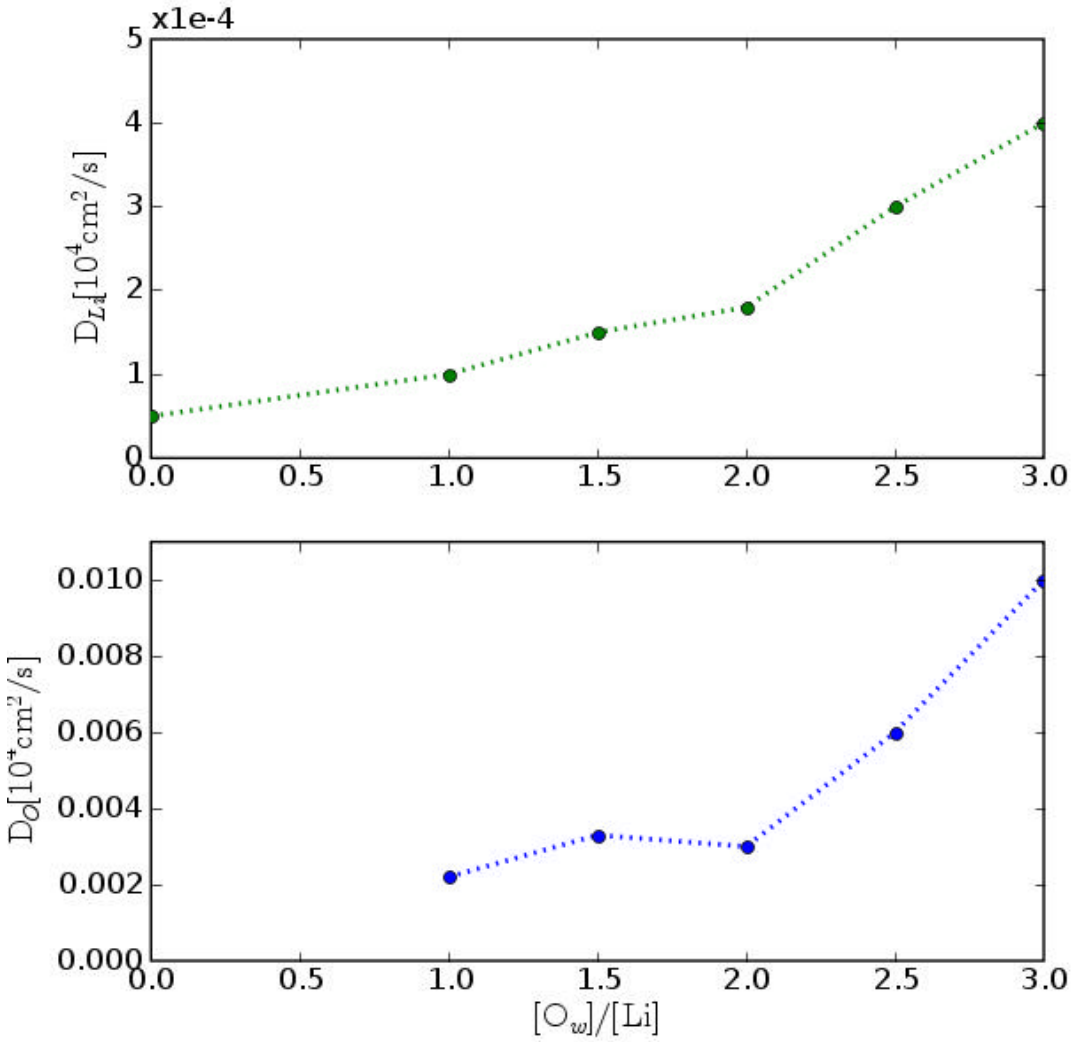

Figure 23: Diffusion coefficient of Li^+ and water oxygen as a function of relative water concentrations

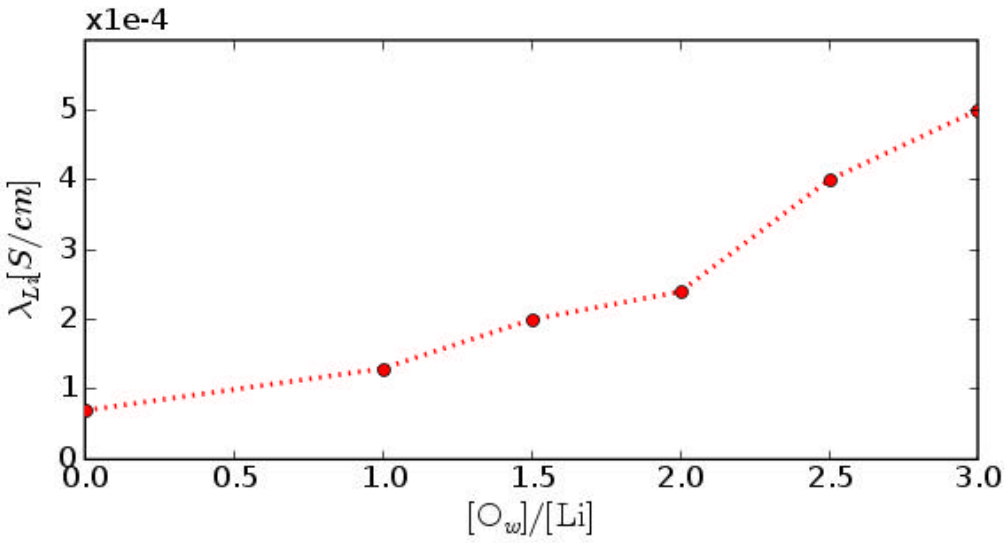

Figure 24: Conductivity of Li+ as a function of relative water concentration

Table 17: Diffusion coefficients of Li^+ and water, and conductivity of Li^+ in studied ternary PEO/LiI/RPOL mixtures plotted in Figures 23 and 24.

$Li:O_E:O_W$	D_{Li} [10^4 cm^2/s]	D_{OW} [10^4 cm^2/s]	λ_{Li} [S/cm]
1:5:0 [a]	0.00005	-	0.00007
1:5:1 [a]	0.0001	0.0022	0.00013
1:5:1.5 [a]	0.0.0015	0.0033	0.00020
1:5:2 [a]	0.00018	0.0030	0.00024
1:5:2.5 [a]	0.0003	0.0060	0.00040
1:5:3 [a]	0.0004	0.010	0.00050
1:1:6.4 [b]	0.0075	0.023	0.0136

To investigate the relationship between the local environment of Li ions and their diffusivity, we analyzed what types of complexes are formed in the solution and how they influence the ionic motion. The complexes were divided into groups according to atoms to which Li is coordinated. The relative numbers of complexes formed in the $I^-:O_E:O_W$ = 1:5:3 solution are shown in Figure 25. It is clearly seen that in the solution of this composition bonding to ether oxygens dominates Li interactions. Also, despite the water concentration being three times higher than I^- ions, complexes including one water molecule are not significantly more probable than those with one I. Somewhat surprisingly, mixed complexes with one O_W, one I^- ion, and two O_E are formed relatively easily. This suggests that it is much easier for water to bind to a Li complex where one O_E has already been replaced, reflecting the relatively smaller stability of such complexes compared to those with four O_E, which are stabilized by the chelate effect. On the other hand the I^- ion itself is not easily replaced by

a water molecule.

Figure 26 presents the mean square displacements of Li^+ ions in different complexes. Due to the limited number of Li^+ ions in the simulation box and low probability of certain complexes, the statistical properties of the results are not good enough to make quantitative conclusions. However, we can still estimate the main trends that determine the ion conduction and other dynamical properties. First of all, we notice that the Li diffusion (corresponding to the mean square displacement) is fastest for the environment with three ether and one water oxygen nearest neighbors. On the other hand the complex with two ether oxygens and two I ions does not move at all during its lifetime. In this particular case there was only a singe complex of this type in the simulation box and it survived for about 600ps. The diffusivity of Li bonded to four ether oxygens is slower than the average diffusivity but is still about twice as fast as that seen in pure PEO melt. The transient complexes with more or less than four coordinated atoms are not shown in this figure because of the poor statistics, which is due to their relative scarcity and short lifetime, but they significantly contribute to the total diffusivity as they are usually formed as part of larger reconfigurations not clearly captured in the figure.

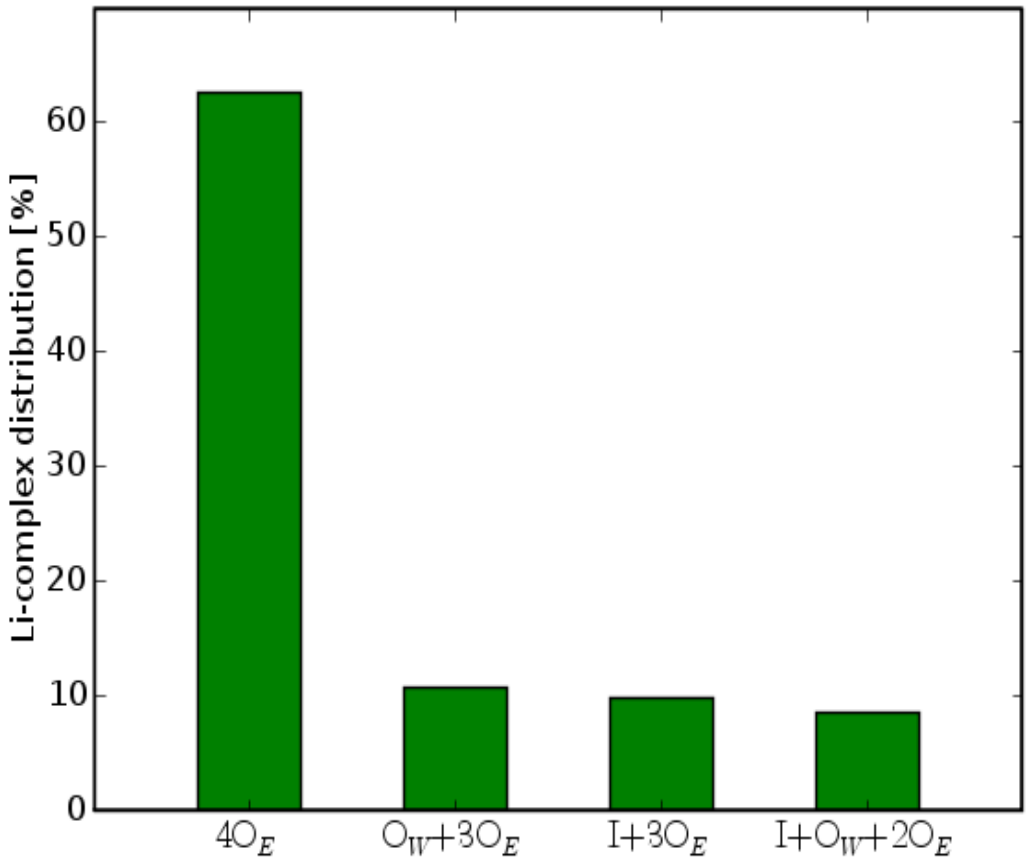

Figure 25: Relative distribution of the most common types of lithium complexes. Eg., 'I + O_W + $2O_E$ ' denotes a lithium complex with one iodide, one water oxygen, and two ether oxygens. Only complexes whose probability is greater than 3% are shown

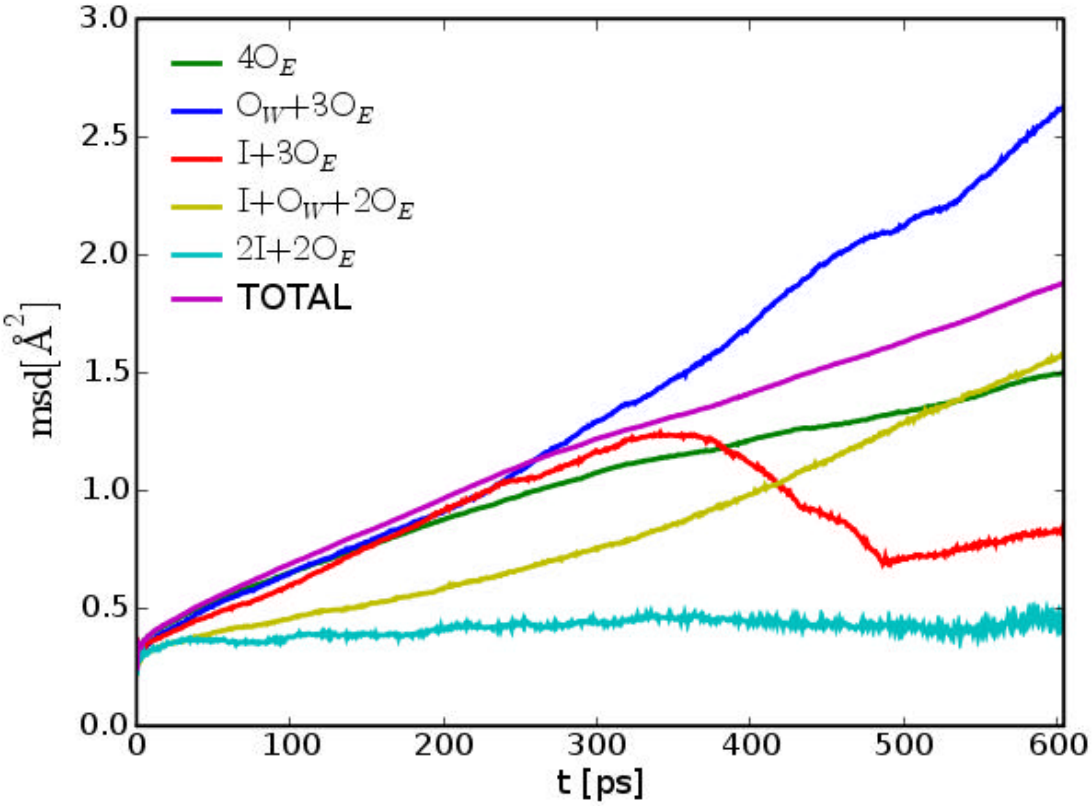

Figure 26: Mean square displacements for various types of most common lithium complexes. The results are only qualitative as the statistics of the measurement often relies on single complexes in the simulation box.

We can see that the effect of water on the diffusivity is threefold: (i) it changes the structure of PEO, increasing diffusion of Li^+ ions even without direct contact with water, (ii) complexes containing a water molecule are more mobile, probably due to the more flexible clusters of water molecules compared to long PEO chains, and (iii) water helps separate Li^+ ions from heavy I^- counterions.

CHAPTER V

5 CONCLUSIONS AND FUTURE WORK

5.1 Summary of the current work

Encouraged by recent experiments with solid polymer electrolytes in aqueous solution, we have performed molecular dynamics simulations and shown their potential as a tool for the investigation of the changes in the environment and conductivity of lithium ions when water is added as a third component. We have demonstrated the importance of polarizability for an accurate simulation of PEO-based polymer electrolytes by comparing the results from three different types of potential models and differ in their treatment of polarization effects (Section 4.3). We found that polarizability cannot be neglected for the accurate calculation of interactions between all components and for the correct prediction of the structural properties of polymer electrolytes (section 4.3). Therefore, for the simulations of a ternary mixture composed of polymer electrolytes in water, we included atomic polarizabilities into our forcefields in the form of the dynamic shell model (Section 4.5). We also performed quantum chemistry calculations to optimize potential parameters used for interactions between PEO and water (Section 4.4). The accuracy of the obtained parameters has been

verified and confirmed by the comparison of simulations and experimentally measured density and excess volume data for water-DME mixtures spanning the full range of relative concentrations (figure 14).

Our molecular dynamics predictions of the structures surrounding lithium ions in PEO aqueous solution are in a good agreement with neutron scattering data at the same conditions (Section 4.5). The simulations also predicted correctly that at high water concentrations lithium ions will prefer to be in an aqueous environment over binding to polymer chains and gave the correct number of water molecules coordinated in the first hydration shell, as was extracted from experiment [11, 21]. Other results presented here have shown that adding low concentrations of PEO polymer molecules to lithium-salt aqueous solution does not significantly influence the hydration of lithium ions, with most of them still coordinated to water (Section 4.5). This can be explained by high solubility of ions in water as a result of its high dielectric constant. This finding agrees well with previous experimental research on the PEO/salt and PEO/water mixtures. It was also found that despite the relatively weaker interaction between ions and individual ether oxygens, PEO can still compete with water due to the stabilizing chelate effect (section 4.5). At lower water concentrations not exceeding ether oxygen concentration by a large amount, which are more interesting from the practical point of view, lithium binds almost exclusively to the polymer molecules. Despite lithium coordination similar to

anhydrous solid polymer electrolytes, addition of water rapidly increases ionic conductivity. However, to reach ionic conductivity comparable to water solutions (LiI/H_2O) the mechanism of ion diffusion must qualitatively change. For this to happen, the amount of water must be considerably increased so that it fully saturates PEO oxygens and provides more flexible water-like environment for ion conduction (section 4.5).

5.2 Future work

Until now, the major limitation of PEO-based polymer batteries is their very low conductivity at room temperatures, which is due to only a small fraction of PEO present in the ion-conducting amorphous phase. However, as it has been reported by experimentalists [11] and observed in our simulations with the optimized polarizable forcefield, the electrical conductivity of the polymer complexes increases with increasing relative humidity. We have seen that water alters the conformation of polymer chains and the ion diffusion mechanism. Since we have found that dramatically increased conductivity is related to the creation of water domains or clusters around the conducting ions, it is important to investigate further the conditions at which these structures can exist, while retaining the desired mechanical properties of solid polymer electrolytes. Further increases in ion conductivity can be potentially achieved by tuning the

system to the most ‘diffusion efficient’ structures by the optimization of water content, polymer chain length, ion concentration, and the choice of a counter ion. Because this task can, in principle, involve a vast number of combinations, computer simulations (with our improved forcefield) should produce accurate results and additional molecular-level insight.

1. U.S government, *Energy Information Administration report.* international energy annual 2005. http://www.eia.doe.gov/iea/res.html

2. Lewis, N.S., *Renewable energy.* Chemical & Engineering News, 2001. 79(13): p. 278-278.

3. Gray,F.M., *Solid polymer electrolytes: fundamentals and technological applications*. 1991, Scotland, UK: VIH Publishers, Inc.

4. Gray, F.M., *Polymer Electrolytes*, ed. J.A.Connor. 1997, Scotland, UK: The Royal Society of Chemistry.

5. Annis, B.K., et al., *A study of the influence of LiI on the chain conformations of poly(ethylene oxide) in the melt by small-angle neutron scattering and molecular dynamics simulations.* Macromolecules, 2000. 33(20): p. 7544-7548.

6. Bedrov, D., O. Borodin, and G.D. Smith, *Molecular dynamics simulation of 1,2-dimethoxyethane/water solutions. 2. Dynamical properties.* Journal of Physical Chemistry B, 1998. 102(47): p. 9565-9570.

7. Bedrov, D., O. Borodin, and G.D. Smith, *Molecular dynamics simulations of 1,2-dimethoxyethane/water solutions. 1. Conformational and structural properties.* Journal of Physical Chemistry B, 1998. 102(29): p. 5683-5690.

8. Bedrov, D., M. Pekny, and G.D. Smith, *Quantum-chemistry-based forcefield for 1,2-dimethoxyethane and poly(ethylene oxide) in aqueous solution.* Journal of Physical Chemistry B, 1998. 102(6): p. 996-1001.

9. Borodin, O. and G.D. Smith, *Molecular dynamics simulations of poly(ethylene oxide)/LiI melts. 1. Structural and conformational properties.* Macromolecules, 1998. 31(23): p. 8396-8406.

10. Borodin, O. and G.D. Smith, *Molecular dynamics simulations of poly(ethylene oxide)/LiI melts. 2. Dynamic properties.* Macromolecules, 2000. 33(6): p. 2273-2283.

11. Hashmi, S.A., *Influence of water absorption on poly-ethylene oxide-based polymer electrolytes complexed with ammonium, sodium and magnesium perchlorates.* Journal of Materials Science, 1998. 33(4): p. 989-993.

12. Stephan, A.M. and K.S. Nahm, *Review on composite polymer electrolytes for lithium batteries.* Polymer, 2006. 47(16): p. 5952-5964.

13. C. W. Kwon, S. E. Cheon, J. M. Song, H. T. Kim, K. B. Kim, C. B. Shin, and S. W. Kim, *Characteristics of a lithium-polymer battery based on a lithium powder anode,* Journal of Power Sources, 93(1-2): p. 145-150

14. Smith, G.D., R.L. Jaffe, and D.Y. Yoon, *A force-field for simulations of 1,2-dimethoxyethane and poly(oxyethylene) based upon ab-initio electronic-structure calculations on model molecules.* Journal of Physical Chemistry, 1993. 97(49): p. 12752-12759.

15. Lin, B., P.T. Boinske, and J.W. Halley, *A molecular dynamics model of the amorphous regions of polyethylene oxide.* Journal of Chemical Physics, 1996. 105(4): p. 1668-1681.

16. Jaffe, R.L., G.D. Smith, and D.Y. Yoon, *Conformations of 1,2-dimethoxyethane from ab-initio electronic-structure calculations.* Journal of Physical Chemistry, 1993. 97(49): p. 12745-12751.

17. Faucher, J.A., et al., *Glass transitions of ethylene oxide polymers.* Journal of Applied Physics, 1966. 37(11): p. 3962-&.

18. Ivison.M.T, B.L.D., *Water Soluble Resins*. 1962, Reinhold, New York: R.L.Davidson and M.Sittig, Eds.

19. Krishnan, M. and S. Balasubramanian, *Order-disorder transitions and melting in a helical polymer crystal: molecular dynamics calculations of model poly(ethylene oxide).* Chemical Physics Letters, 2004. 385(5-6): p. 351-356.

20. Annis, B.K., Borodin, O. and Smith, G.D., *The structure of a poly(ethylene oxide) melt from neutron scattering and molecular dynamics simulations.* Journal of Chemical Physics, 2001. 115(23): p. 10998-11003.

21. Annis, B.K., Y.S. Badyal, and J.M. Simonson, *Neutron-scattering determination of the Li+ environment in an aqueous poly(ethylene oxide) solution.* Journal of Physical Chemistry B, 2004. 108(8): p. 2554-2556.

22. Brandell.D, *Understanding ionic conductivity in crystalline polymer electrolytes,* in *materials chemistry*. 2005, Uppsals University: Uppsals, Sweden.

23. Gilbert T.Morgan, H.D.K.D., *CLXII.-Researches on residual affinity and co-ordination. Part II. Acetylacetones of selenium and tellurium.* Journal of chemical Society 1920. 117: p. 1456-1465.

24. Borodin, O., G.D. Smith, and R.L. Jaffe, *Ab initio quantum chemistry and molecular dynamics simulations studies of LiPF6/poly(ethylene oxide) interactions.* Journal of Computational Chemistry, 2001. 22(6): p. 641-654.

25. Grujicic, M., et al., *An atomic level analysis of conductivity and strength in poly(ethylene oxide) sulfonic acid-based solid polymer electrolytes.* Materials Science and Engineering B-Solid State Materials for Advanced Technology, 2005. 117(2): p. 187-197.

26. Mullerplathe, F. and W.F. Vangunsteren, *Computer-simulation of a polymer electrolyte - lithium iodide in amorphous poly(ethylene oxide).* Journal of Chemical Physics, 1995. 103(11): p. 4745-4756.

27. Johansson, A., A. Lauenstein, and J. Tegenfeldt, *Effect of water on diffusion and ionic-conductivity in peg and licf(3)so(3)peg(10).* Journal of Physical Chemistry, 1995. 99(16): p. 6163-6166.

28. Wendsjo, A., J. Lindgren, and C. Paluszkiewicz, *Structure, dynamics and morphology in the system m(cf3so3)2 peon for m=zn and pb.* Electrochimica Acta, 1992. 37(9): p. 1689-1693.

29. Lal, J. and I.F. Hakem, *Unusual behaviour of poly(ethylene-oxide) in aqueous mixtures.* European Physical Journal E, 2004. 15(2): p. 217-223.

30. Briscoe, B., P. Luckham, and S. Zhu, *Rheological study of poly(ethylene oxide) in aqueous salt solutions at high temperature and pressure.* Macromolecules, 1996. 29(19): p. 6208-6211.

31. Londono, J.D., Smith, G.D., et al., *Cation environment in molten lithium iodide doped poly(ethylene oxide).* Macromolecules, 1997. 30(23): p. 7151-7157.

32. H.C.Benoit, J.S.H., *Polymers and Neutron Scattering*. 1994: Oxford University Press.

33. Rennie, A.R. and R.C. Oberthur, *Small-angle neutron-scattering on periodically deformed polymers.* Revue De Physique Appliquee, 1984. 19(9): p. 765-768.

34. Bizzarri, A.R., *Neutron scattering and molecular dynamics simulation: a conjugate approach to investigate the dynamics of electron transfer proteins.* Journal of Physics-Condensed Matter, 2004. 16(6): p. R83-R110.

35. Bieze, T.W.N., et al., *Distribution of water around poly(ethylene oxide) - a neutron-diffraction study.* Journal of Physical Chemistry, 1994. 98(26): p. 6568-6576.

36. Dove, M.T., M.G. Tucker, and D.A. Keen, *Neutron total scattering method: simultaneous determination of long-range and short-range order in disordered materials.* European Journal of Mineralogy, 2002. 14(2): p. 331-348.

37. Judeinstein, P., et al., *NMR multi-scale description of ionic conductivity mechanisms inside polymer electrolytes.* Acta Chimica Slovenica, 2005. 52(4): p. 349-360.

38. M.P.Allen, D.J.Tildesley., *Computer Simulations of Liquids*. 1987, London, UK.

39. Wang, W., et al., *Biomolecular simulations: Recent developments in forcefields, simulations of enzyme catalysis, protein-ligand, protein-protein, and protein-nucleic acid noncovalent interactions.* Annual Review of Biophysics and Biomolecular Structure, 2001. 30: p. 211-243.

40. Leach, A., *Molecular Moldeing:Principles and Applications*. 2001: Prentice Hall.

41. Nose, S., *Molecular-dynamics simulations - preface.* Progress of Theoretical Physics Supplement, 1991(103): p. R1-R1.

42. Hoover, W.G., *Canonical dynamics - equilibrium phase-space distributions.* Physical Review A, 1985. 31(3): p. 1695-1697.

43. J.E.Lennard-Jones, *Cohesion.* Proceeding of the physical society, 1931. 43: p. 461-482.

44. Cao, J.S. and B.J. Berne, *Theory and simulation of polar and nonpolar polarizable fluids.* Journal of Chemical Physics, 1993. 99(9): p. 6998-7011.

45. Chialvo, A.A. and P.T. Cummings, *Simple transferable intermolecular potential for the molecular simulation of water over wide ranges of state conditions.* Fluid Phase Equilibria, 1998. 151: p. 73-81.

46. Chialvo, A.A., et al., *Thermodynamics and kinetics of ion speciation in supercritical aqueous solutions: a molecular-based study.* Fluid Phase Equilibria, 1998. 151: p. 107-115.

47. Chialvo, A.A., et al., *Solvation in supercritical electrolyte solutions. Formal and experimental results.* Abstracts of Papers of the American Chemical Society, 1998. 215: p. U204-U204.

48. Predota, M., P.T. Cummings, and A.A. Chialvo, *Pair approximation for polarization interaction: efficient method for Monte Carlo simulations of polarizable fluids.* Molecular Physics, 2001. 99(4): p. 349-354.

49. Sprik, M, Klein, M.L., *A polarizable model for water using distributed charge sites,* Journal of Chemical Physics, 1988, 89

50. Jorgensen, W.L., *Quantum and statistical mechanical studies of liquids .24. revised tips for simulations of liquid water and aqueous-solutions.* Journal of Chemical Physics, 1982. 77(8): p. 4156-4163.

51. Car, R. and M. Parrinello, *Unified approach for molecular-dynamics and density-functional theory.* Physical Review Letters, 1985. 55(22): p. 2471-2474.

52. Paricaud, P., et al., *From dimer to condensed phases at extreme conditions: Accurate predictions of the properties of water by a Gaussian charge polarizable model.* Journal of Chemical Physics, 2005. 122(24).

53. Yu, H.B. and W.F. van Gunsteren, *Accounting for polarization in molecular simulation.* Computer Physics Communications, 2005. 172(2): p. 69-85.

54. Thole, B.T., *Molecular polarizabilities calculated with a modified dipole interaction.* Chemical Physics, 1981. 59(3): p. 341-350.

55. Mitchell, P.J. and D. Fincham, *Shell-model simulations by adiabatic dynamics.* Journal of Physics-Condensed Matter, 1993. 5(8): p. 1031-1038.

56. Borodin, O. and G.D. Smith, *Development of quantum chemistry-based forcefields for poly(ethylene oxide) with many-body polarization interactions.* Journal of Physical Chemistry B, 2003. 107(28): p. 6801-6812.

57. I.T.Todorov, W.S., *The DL_POLY_2 user manual*. 2006, Cheshire, HK: CCLRC Daresbury Laboratory.

58. Stilling.FH and A. Bennaim, *Liquid-vapor interface potential for water.* Journal of Chemical Physics, 1967. 47(11): p. 4431-&.

59. Koneshan, S., J.C. Rasaiah, and L.X. Dang, *Computer simulation studies of aqueous solutions at ambient and supercritical conditions using effective pair potential and polarizable potential models for water.* Journal of Chemical Physics, 2001. 114(17): p. 7544-7555.

60. Lamoureux, G., A.D. MacKerell, and B. Roux, *A simple polarizable model of water based on classical Drude oscillators.* Journal of Chemical Physics, 2003. 119(10): p. 5185-5197.

61. Berendsen, H.J.C., J.R. Grigera, and T.P. Straatsma, *The missing term in effective pair potentials.* Journal of Physical Chemistry, 1987. 91(24): p. 6269-6271.

62. Ahlstrom, P., et al., *A molecular-dynamics study of polarizable water.* Molecular Physics, 1989. 68(3): p. 563-581.

63. Dang, L.X., *The nonadditive intermolecular potential for water revised.* Journal of Chemical Physics, 1992. 97(4): p. 2659-2660.

64. Smith, G.D., O. Borodin, and D. Bedrov, *A revised quantum chemistry-based potential for poly(ethylene oxide) and its oligomers in aqueous solution.* Journal of Computational Chemistry, 2002. 23(15): p. 1480-1488.

65. Borodin, O., G.D. Smith, and R. Douglas, *Forcefield development and MD simulations of poly(ethylene oxide)/LiBF4 polymer electrolytes.* Journal of

Physical Chemistry B, 2003. 107(28): p. 6824-6837.

66. Stout, J.M. and Dykstra, C.E., *Static dipole polarizabilities of organic molecules. Ab initio calculations and a predictive model.* Journal of the american chemical society, 1995. 117(18): p. 5127-5132.

67. Borodin, O., D. Bedrov, and G.D. Smith, *A molecular dynamics simulation study of polymer dynamics in aqueous poly(ethylene oxide) solutions.* Macromolecules, 2001. 34(16): p. 5687-5693.

68. Smith, G.D., D. Bedrov, and O. Borodin, *Molecular dynamics simulation study of hydrogen bonding in aqueous poly(ethylene oxide) solutions.* Physical Review Letters, 2000. 85(26): p. 5583-5586.

69. Trouw, F., et al., *Diffusion in aqueous solutions of 1,2-dimethoxyethane: comparison of molecular dynamics simulations and quasielastic neutron scattering.* Chemical Physics, 2000. 261(1-2): p. 137-148.

70. Trouw, F.R., et al., *Quasielastic neutron-scattering study of the local dynamics of poly(ethylene glycol) dimethyl ether in aqueous solution.* Journal of Physical Chemistry B, 2003. 107(38): p. 10446-10452.

71. Bedrov, D. and G.D. Smith, *Molecular dynamics simulations of 1,2-dimethoxypropane and 1,2-dimethoxyethane in aqueous solution.* Journal of Physical Chemistry B, 1999. 103(45): p. 10001-10006.

72. Bedrov, D., et al., *Simulation and QENS studies of molecular dynamics in aqueous solutions of 1,2-dimethoxyethane.* Journal of Physical Chemistry B, 2000. 104(21): p. 5151-5154.

73. Smith, G.D., R.L. Jaffe, and H. Partridge, *Quantum chemistry study of the interactions of Li+, Cl-, and I- ions with model ethers.* Journal of Physical Chemistry A, 1997. 101(9): p. 1705-1715.

74. Ryckaert, J.P., Ciccotti, G., Berendsen, H.J.C., *Numerical-jntegration of cartesican equations of motion of a system with constraints-molecular-dynamics of n-alkanes.* Journal of Computational Physics, 23(3): p. 327-341.

75 Borodin, O. and G.D. Smith, *Molecular dynamics simulation study of*

LiI-doped diglyme and poly(ethylene oxide) solutions. Journal of Physical Chemistry B, 2000. 104(33): p. 8017-8022.

76. Shi, J. and C.A. Vincent, *The effect of molecular-weight on cation mobility in polymer electrolytes.* Solid State Ionics, 1993. 60(1-3): p. 11-17.

77. Shi, J., and Vincent, C. A, *The effect of molecular weight on cation mobility in polymer electrolytes.* Solid State Ionics, 1993(60): p. 11-17.

78. Yamaguchi, T., et al., *Structure and dynamics of supercooled and glassy aqueous ionic-solutions.* Journal of Molecular Liquids, 1995. 65-6: p. 91-98.

79. Howell, I. and G.W. Neilson, *Li+ hydration in concentrated aqueous solution.* Journal of Physics-Condensed Matter, 1996. 8(25): p. 4455-4463.

80. Dang, L.X., *Temperature-dependence of interactions of an ion-pair in water - a molecular-dynamics study.* Journal of Chemical Physics, 1992. 97(3): p. 1919-1921.

81. Dang, L.X., *Development of nonadditive intermolecular potentials using molecular-dynamics - solvation of li+ and f- ions in polarizable water.* Journal of Chemical Physics, 1992. 96(9): p. 6970-6977.

82. Gai, H.D., et al., *Quantum statistical mechanical simulation of the ion-water cluster I-(H2O)(n): The importance of nuclear quantum effects and anharmonicity.* Journal of Chemical Physics, 1996. 105(19): p. 8835-8841.

83. Tao, Z. and P.T. Cummings, *Molecular dynamics simulation of inorganic ions in PEO aqueous solution.* Molecular Simulation, 2007. 33(15): p. 1255-1260.

84. Hakem, I.F., J. Lal, and M.R. Bockstaller, *Mixed solvent effect on lithium-coordination to poly(ethylene oxide).* Journal of Polymer Science Part B-Polymer Physics, 2006. 44(24): p. 3642-3650.